

DIPLOMARBEIT / DIPLOMA THESIS

Titel der Diplomarbeit / Title of the Diploma Thesis

„Structure based pharmacophore modeling of
mitochondrial respiratory complex III“

verfasst von / submitted by

Claudia Seifried

angestrebter akademischer Grad / in partial fulfilment of the requirements for the degree of
Magistra der Pharmazie (Mag.pharm.)

Wien, 2021 / Vienna, 2021

Studienkennzahl lt. Studienblatt /
degree programme code as it appears on
the student record sheet:

UA 449

Studienrichtung lt. Studienblatt /
degree programme as it appears on
the student record sheet:

Diplomstudium Pharmazie

Betreut von / Supervisor:

Univ.-Prof. Mag. Dr. Gerhard F. Ecker

Acknowledgement

First of all, I would like to express my greatest thanks to Univ.-Prof. Mag. Dr. Gerhard F. Ecker, who made it possible for me to be part of "Pharmacoinformatics Research Group" team in the Department of Pharmaceutical. It was a new and great challenge to apply the knowledge acquired during the pharmacy study in a scientific work. Thanks to many years of experience and the wide knowledge of Prof. Ecker, I always felt supported and cheered up when things didn't work as planned.

In general, there was a very open and familiar relationship in the team which means that you never felt alone and always felt comfortable.

My Co-supervisor Florentina Troger always supported me with her advices which made a great contribution to finish my diploma thesis.

I also express gratitude to all my work colleagues in "Apotheke Altmannsdorf", especially Mag. Thomas Halak and Mag. Lukas Mayerhofer, who always supported me with understanding and tolerance and thereby helped me to achieve my goal. I am now looking forward to further cooperation and new challenging fields of work.

I wish to extend special thanks to my parents, sister, brother and also to my friends Aylin, Melanie, Sabrina, who supported me in every desperate situation and kept me motivated to persevere.

Last but not least, I want to thank all of my lovely student colleagues, especially Sigrid, Marie, Vicky, Anna and Natalie, with whom I could laugh together despite desperate moments at lab days and lectures on the university and who I could always rely on.

Now at the end of the way, I proudly share this success and joy with my beloved ones.

Thank you all for the support and the belief in me!

Table of contents

1	Abstract	VI
2	Zusammenfassung	VII
3	Introduction	1
3.1	<i>Mitochondria</i>	1
3.2	<i>Respiratory chain</i>	1
3.2.1	Cytochrome bc ₁ complex	2
3.3	<i>Inhibitors of bc1-Complex</i>	5
4	Aim of the thesis	6
5	Material and Methods	7
5.1	<i>Data Collection</i>	7
5.1.1	Protein Data Bank	7
5.1.2	Promals 3D	17
5.1.3	Uniprot	17
5.1.4	Drugbank	17
5.2	<i>Docking Studies</i>	17
5.2.1	Software	18
5.3	<i>Pharmacophore modeling</i>	19
5.3.1	Software	19
5.4	<i>Knime Workflow</i>	20
5.4.1	Pareto Ranking	20
6	Results and Discussion	21
6.1	<i>Docking</i>	26
6.1.1	Glide Docking Experiments	26
6.1.2	Induced-fit Docking Experiments	29
6.2	<i>Pharmacophore modeling</i>	31
6.2.1	Qo-Site	31

6.2.2 Qi-Site	33
6.3 <i>Knime Workflow</i>	34
7 Conclusion	38
8 References	39
9 Appendix	43
9.1 <i>List of Figures</i>	43
9.2 <i>List of Tables</i>	43
9.3 <i>List of Abbreviations</i>	44

1 Abstract

Mitochondria are important cell organelles that supply the organism with energy. Important metabolic processes take place in them. The diploma thesis is about the mitochondrial complex III of the respiratory chain.

Within the last years, several crystal structures of various species have been solved with inhibitors. The protein consists of three catalytic units, whereby an extrinsic domain, the so-called ISP, can assume different positions. There are two binding sites in cytochrome b, which divide the electron transfer into two pathways, the Qo-side and Qi-side. These two active centers work together for the formation of ATP and the different conformations of ISP allow further classifications into three groups of inhibitors. If the important redox reactions of mitochondria are interrupted, it can lead to mitochondrial dysfunction and diseases such as cancer or other metabolic disorders. In the last decade, in silico models have generally increased and gained in importance. A lot of studies exist that have explained co-crystallized bc1-complexes with the binding mode of inhibitors in bovine and chicken complexes. An already existing crystal structure of the human complex render possible to run induced-fit docking approaches in the human complex, which has a high sequence identity with the bovine and chicken complexes. Subsequently, pharmacophore modeling helped to evaluate the docking experiments and the results were linked and evaluated with the machine learning platform Knime.

Finally, a list of drugs with potential mitochondrial toxicity was created for further experiments.

2 Zusammenfassung

Diese Arbeit beschäftigte sich mit dem mitochondrialen Komplex III der Atmungskette. Die Mitochondrien sind wichtige Zellorganellen, die dem Organismus als Energielieferant dienen und in denen wichtige Stoffwechselprozesse stattfinden.

Das Protein besteht aus drei katalytischen Einheiten, wobei eine extrinsische Domäne, das sog. ISP, verschiedene Stellungen einnehmen kann. Das Cytochrom b weist zwei Bindungsstellen auf, durch die der Elektronentransfer aufgeteilt wird. Durch diese Aufteilung in zwei aktive Zentren und der unterschiedlichen Konformation des ISP können drei Klassifizierungen der Inhibitoren erfolgen.

Werden in den Mitochondrien diese wichtigen Redoxreaktionen unterbrochen, kann dies zu mitochondrialen Dysfunktionen und Erkrankungen wie Krebs und Stoffwechselstörungen führen. Um solche Nebenwirkungen von Arzneimitteln frühzeitig zu erkennen, werden mittlerweile Computer-unterstützte Analysen durchgeführt. In der Forschung haben in den letzten Jahren *in silico* Modelle zugenommen und an Wichtigkeit gewonnen.

In den letzten Jahren wurden einige Kristallstrukturen von verschiedenen Spezies mit Inhibitoren und deren Bindungsmodus aufgeklärt.

Eine bereits vorhandene Kristallstruktur des humanen Komplexes, der eine hohe Sequenzähnlichkeit mit den Rindern oder Hühner Komplexen aufweist, erlaubte auch im humanen Komplex induced-fit Docking Versuche durchzuführen.

Anschließend durchgeführte Pharmakophor Erstellung half bei der Evaluierung der Docking Experimente. Die Auswertung der Ergebnisse erfolgte mit Hilfe maschinellen Lernens mit der Plattform Knime.

Schlussendlich entstanden Listen mit potenziellen Arzneimitteln, die eine mitochondriale Toxizität aufweisen und in weiteren Experimenten ausgewertet werden können.

3 Introduction

3.1 Mitochondria

Mitochondria are the “energy factory” of eucaryotic cells, that produce Adenosin-triphosphate, the most important fuel of many reactions. They have an outer membrane, inner membrane and between them is Intermembrane space. The inner membrane has Cristae, which expands the surface of the inner mitochondrial membrane, enhancing its ability to produce ATP.

The mitochondria not only serve as a supplier of energy, but also have other functions, such as storing calcium¹, initiating apoptosis² and synthesizing iron-sulfur clusters³. The last one is also an important element for some complexes of cellular respiration. Their remarkable role in many areas of cell functions and cell communication also results in their great importance in the development of diseases such as cancer, neurological diseases and metabolic diseases.⁴

3.2 Respiratory chain

One of the most important function of the mitochondria is the respiratory chain. There are 4 transmembrane proteins, located in the inner membrane, which produce a transmembrane proton electrochemical gradient as result of the redox reactions.

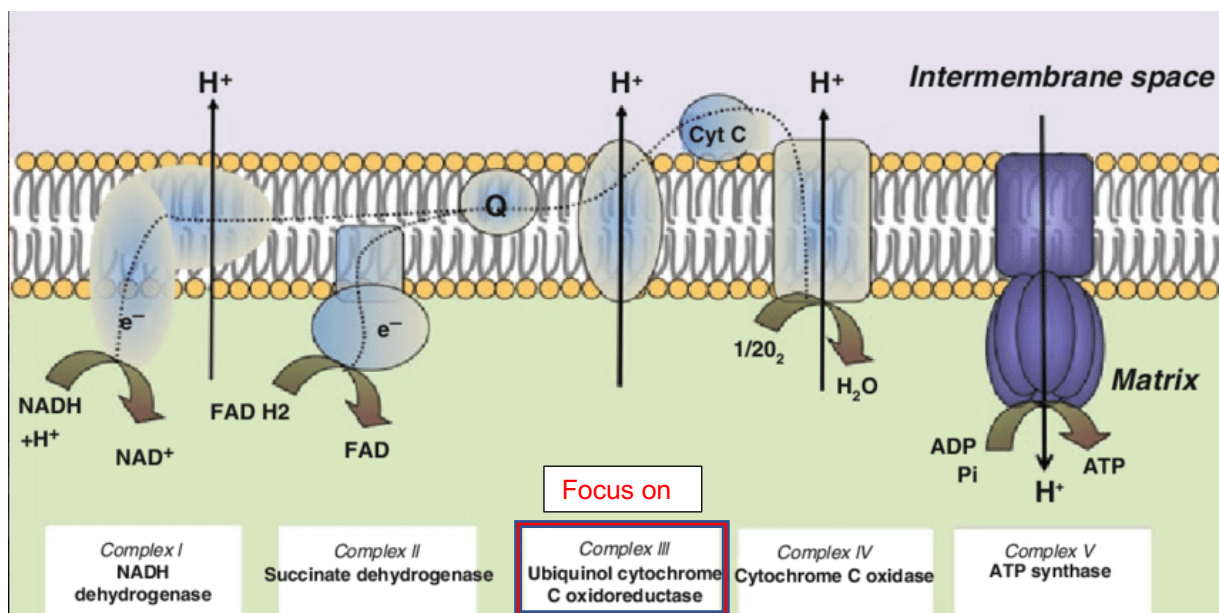


Figure 1: Complexes of the mitochondrial Respiratory chain⁵

Each protein complex accepts the electrons and complexes I, III and IV use the energy to pump protons into the intermembrane space from the mitochondrial matrix. The resulting transmembrane proton gradient is used to make Adenosintriphosphate (ATP) via ATP-synthase.^{2,6}

3.2.1 Cytochrome bc₁ complex

The focus of my thesis is on cytochrome bc₁ complex, also called Ubiquinole-cytochrome-C-oxidoreductase or simply Complex III.

It is a dimer with 22 chains and each monomer contains 11 subunits in eukaryotes. There are three following essential catalytic units with prosthetic groups, cytochrom c (yellow ribbon) with one heme c; cytochrome b (green and blue ribbon) with two hemes (low potential bL and high potential bH); and Rieske Protein with the Iron-sulfur-center (red ribbon).⁷

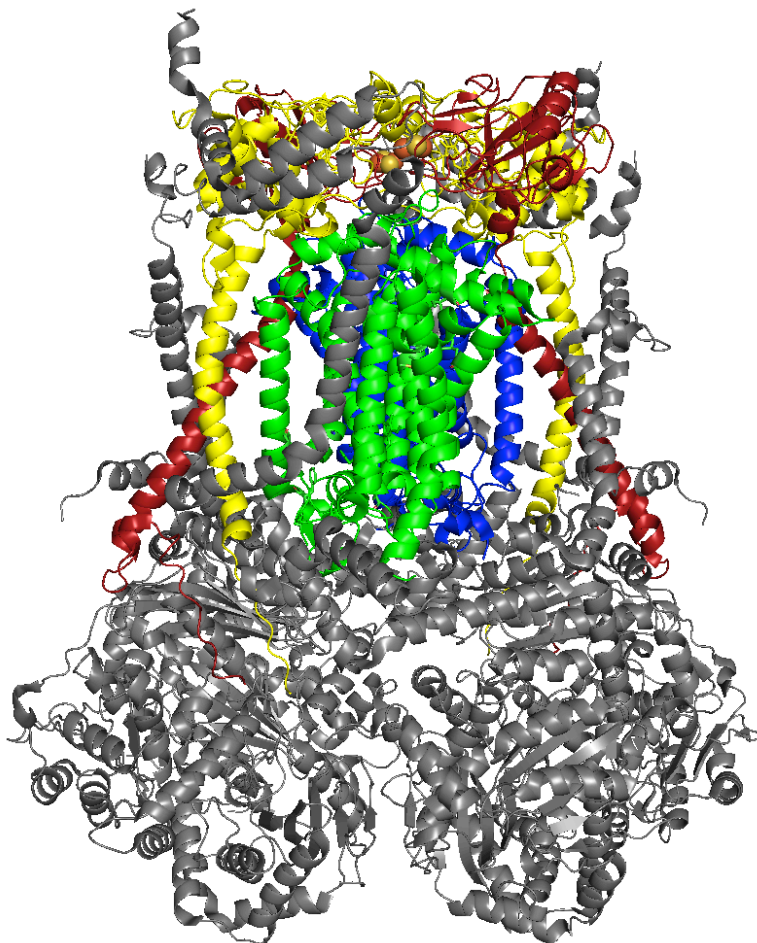


Figure 2: human dimer bc₁-complex with the three essential catalytic

Color code: green → J-chain of cytochrome b; blue → V-chain of cyt. b; yellow → cytochrome c; red → ISP

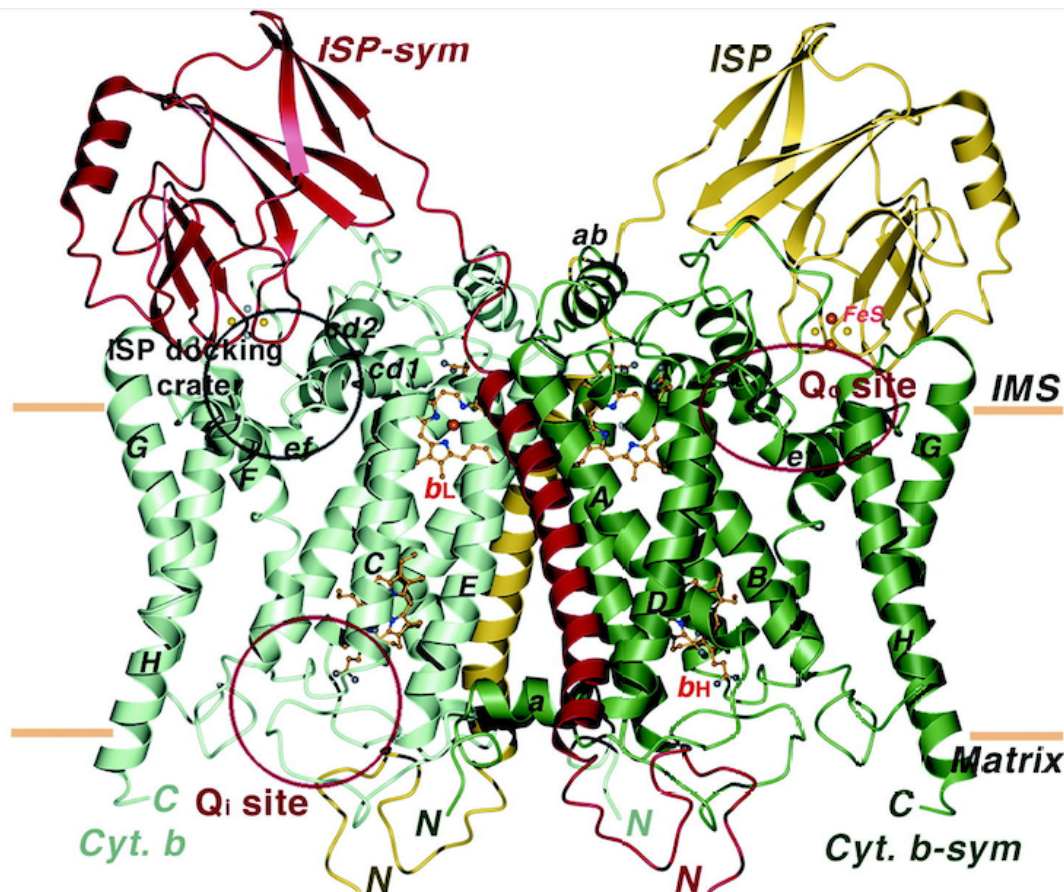


Figure 3: View of the dimeric cyt b and ISP in the bc1-complex⁷

There are eight transmembrane helices, which are named sequentially from A to H. The two b-type hemes are labeled bL and bH. Also, the two binding pockets Q_o and Q_i are displayed. The ISP docking crater is also shown, where the interaction between ISP and cyt. b takes place.

The subunit cytochrome b, in which the binding sites Q_o and Q_i are located, is anchored in the membrane with eight transmembrane helices. The subunits cytochrome c1 and ISP are only embedded in the membrane with one transmembrane helix. A difference between the head domains of cyt c1 and ISP is that cyt c1 is rigid and flexibility is possible in the extrinsic ISP domain.⁷

The two active centers for the redox reaction are shown in Figure 4 as Q-Cycle mechanism. It also depicts three examples of inhibitors for each binding mode.

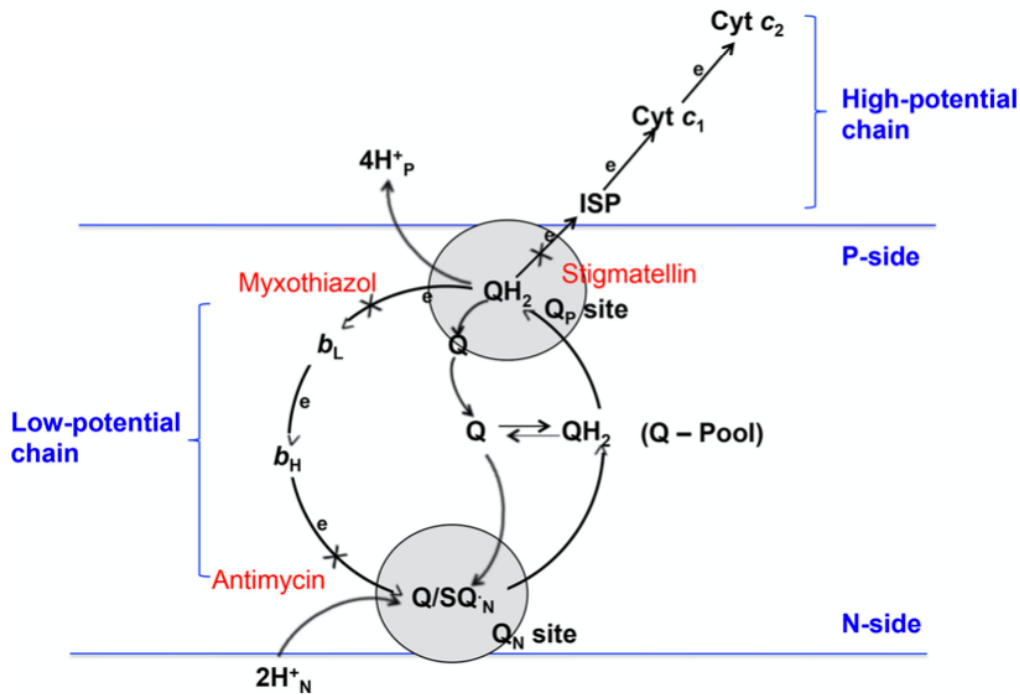


Figure 4: Q-cycle mechanism ⁸

It shows the ubiquinol (QH_2) oxidation site near to the positive membrane side, referred to as $\text{Q}_{o/p}$ site, and the ubiquinone (Q) reduction site near to the negative membrane side, also known as $\text{Q}_{i/N}$ site.

Q_o stands for “outer membrane” or Q_p for “positive side” and Q_i denotes “inner membrane” or Q_N for “negative side”.

Ubiquinone is reduced to ubiquinol/ubihydroquinone (QH_2) by complexes I and II by accepting two electrons and protons.

Then ubiquinol diffuses to complex III where the quinol oxidation bifurcates into two separate pathways.

First, ubiquinol binds to the Q_o -site and transfers an electron via the iron-sulfur and heme c to Cytochrome c. The result is a ubiquinone semimolecule (Q^\cdot), which is unstable and oxidizes to ubiquinone (Q) when one more electron is released. Then this electron flows via heme b_L and heme b_H to the Q_i -site, where it will be absorbed by an ubiquinone molecule and which is thereby stored as semiquinone. In this first half cycle, two hydrogen atoms are pumped into the intermembrane space.

In the second cycle, an ubiquinol (QH_2) binds again and the electron transfer takes place analogously, with the ubiquinol being regenerated at the Q_i center and released back into the Q-pool.

In summary two electrons are transferred from ubiquinol to cytochrome c, two protons were removed from the matrix and then four protons were released into the intermembrane space.⁸⁻¹⁰

3.3 Inhibitors of bc1-Complex

The classification of the inhibitors can be divided into three groups by the two active centers. Class P binds to the $Q_{o/P}$ side, class N to the $Q_{i/N}$ side and class PN binds to both places. In some studies, it is reported that the electron transfer leads to a change in conformation of the protein, whereby a movement of the iron-sulfur protein is observed.^{7,8} This determination of the mobile iron-sulfur domain allowed a more specific subdivision of the inhibitor classes for the $Q_{o/P}$ site. Depending on the conformation of ISP, the class P can split in P_m , mobile conformation, and P_f , fixed conformation, groups. A place above the Q_o pocket is called ISP docking crater, where the the extrinsic domain can temporarily bind via His161.⁷

The inhibitors stigmatellin, UHDBT, and famoxadone stabilize the ISP domain, so they are assigned to the P_f class.⁷ The Class P_m includes myxothiazole, MOAS and Azoxystrobin, which ensure the mobilization of the ISP region.⁷

NQNO¹¹ and Ascochlorin¹² are examples of ligands, who can bind in both pockets.

4 Aim of the thesis

In the last few years, the term “in silico” has become more and more important in science. Computer-based research is gaining more priority, which means that possible adverse effects can be identified at an early stage. Biochemical, pharmacological and toxicological processes are virtually simulated and analyzed. It ensures more safety for clinical studies and certainly reduction in animal experiments.

The aim of my diploma thesis was to identify substances that show mitochondrial toxicity via inhibition of the respiratory complex and possibly to further evaluate them experimentally. The computational work was structure based, using software for docking experiments and pharmacophore modeling.

There are many co-crystallized structures from bos taurus and gallus gallus organism with ligands on PDB accessible, which were tested by redocking experiments. The ligands were also analyzed in the human complex by induced-fit docking. In the next step, structure-based pharmacophore modeling was conducted.

Finally, a virtual screening was performed with a data set from Drugbank and evaluated by using a Knime workflow.

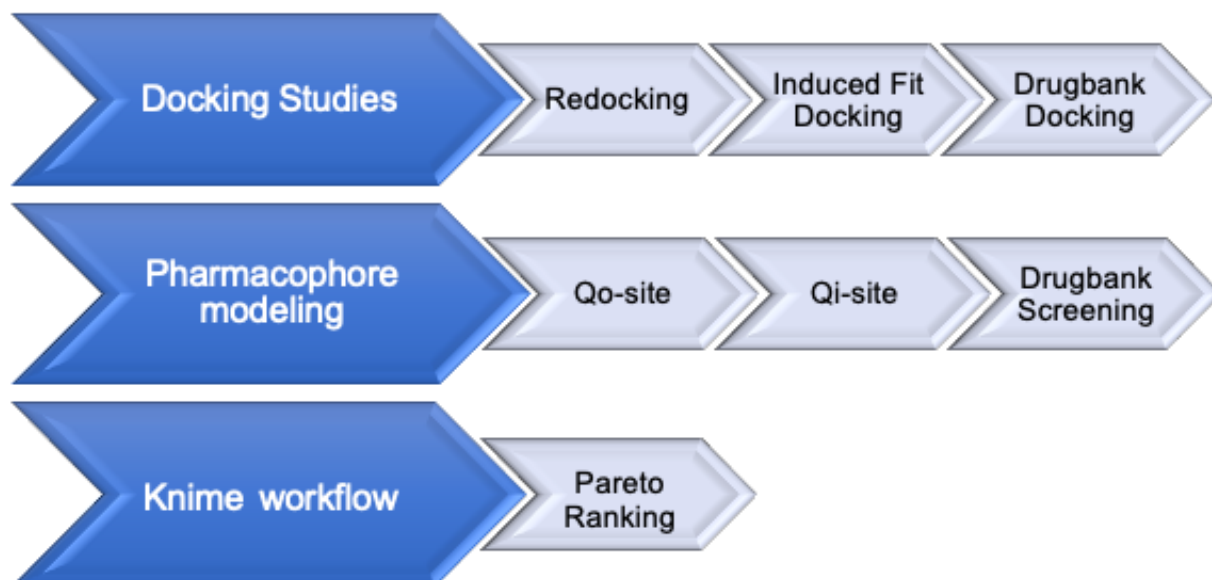


Figure 5: Steps of the Thesis

5 Material and Methods

5.1 Data Collection

5.1.1 Protein Data Bank

Protein Data Bank (PDB) provides access to 3D structural data of large biological molecules including Proteins, nucleic acids and complex assemblies. X-ray is one of the most important methods for structure analyses, followed by NMR-spectroscopy and electron microscopy.¹³

There are many crystal structures available for the mitochondrial protein bc1-complex. In the following tables all PDBs of the various species *Bos taurus* (Table 1), *Gallus gallus* (Table 2), and *Sacharomyces cerevisiae* (Table 3) are summarized. Some important interactions of the inhibitors with the side chains of the binding pocket from the bovine complex, that have been described in studies, are also listed.

<u>Inhibitor</u>	<u>PDB</u>	<u>H-bond Interaction</u>	<u>other Interactions</u>	<u>Method</u>	<u>Resolution</u>
Qo-Site					
Azoxystrobin ⁷	1SQB	Glu271	Met124 Phe128 Tyr131 Ile46 Pro270 Phe274 Ala277 Leu294 Ile298	X-Ray	2.69 Å
Myxothiazol ⁷	1SQP	Glu271 Tyr273	Ala127	X-Ray	2.7 Å
Stigmatellin A ⁷	1SQX 2A06 1PP9	Glu271	Met124 Ala125 Met129 Ile146 Pro270 Ohe274 Leu294	X-Ray	3.0 Å 2.1 Å 2.1 Å

MOAS ⁷	1SQQ	Glu271	Gly142 Ile146 Pro270	X-Ray	3.0 Å
UHDBT ⁷	1SQV	Tyr131	Met124 Val145 Pro270 Tyr273 Phe274	X-Ray	2.85 Å
Famoxadone ¹⁴	1L0L	Glu271	Phe91 Met124 Gly142 Ile146 Tyr131 Tyr273 Tyr278	X-Ray	2.35 Å
Fenamidone ⁸	5KLV			X-Ray	2.65 Å
Stigmatellin A + Antimycin ¹⁵	1PPJ			X-Ray	2.1 Å
JG144 ¹⁶	2FYU			X-Ray	2.26 Å
Qi-Site					
Antimycin A ¹¹	1NTK	Ser35 ° Asp228 ^	Phe220 ° Leu197 ° Ile27 ° Trp31 ^ Gly38 Met190	X-Ray	2.6 Å
NQNO ¹¹	1NU1	Ser205	Phe220 ° His201 ^ Asp228 ^ Leu200 ^ Tyr224 Lys227	X-Ray	3.2 Å
SCR0911 ¹⁷	5OKD	Ser35 °	Phe220 °	X-Ray	3.1 Å

	6FO6	His201 ^	Asp228 ^ Ser205	CryoEM	4.1 Å
MJM170 ¹⁸	5NMI		Ser35 ° His201 ^ Phe220 ° Asp228 ^ Ser205 ° Pro24 ^ Ile27 Trp31 Ile39 Ile42 Phe18	X-Ray	3.5 Å
GSK932121 ¹⁷	6FO0 4D6U			CryoEM X-Ray	4.1 Å 3.1 Å
GW844520 ^{19,20}	4D6T			X-Ray	3.57 Å
WDH2G7 ²¹	6HAW			X-Ray	3.45 Å

Table 1: Crystal structures of bos taurus bc1-complex with inhibitors divided in the two binding site modes

Legend of the Table 1:

° conserved residues in all species

^ conserved residues in bovine, chicken and human bc1-complex

<u>Inhibitor</u>	<u>PDB</u>	<u>Method</u>	<u>Resolution</u>
Qo-site			
Azoxystrobin	3L71	X-Ray	2.84 Å
Famoxadone	3L74	X-Ray	2.76 Å
MOA ²²	3TGU	X-Ray	2.7 Å
Fenamidone	3L75	X-Ray	2.79 Å
Stigmatellin	3H1J 2IBZ 2BCC	X-Ray	3.0 Å
Kresoxym-l-dimethyl	3L72	X-Ray	3.06 Å

Crocacin A, CrocacinD (idoinated)	3CWB	X-Ray	3,51 Å
Triazolone	3L73	X-Ray	3.04 Å
Trifloxystrobin	3L70	X-Ray	2.75 Å
Qo + Qi-site			
Stigmatellin + Antimycin ²³	3BCC	X-Ray	3.7 Å
	3H1I		3.53 Å
Ascochlorin ²⁴	3H1L	X-Ray	3.21 Å

Table 2: Crystal structures of Gallus gallus bc1-complexe with inhibitors

<u>Inhibitor</u>	<u>PDB</u>	<u>Method</u>	<u>Resolution</u>
Qo-site			
Atovaquone	4PD4	X-Ray	3.04 Å
Stigmatellin	2IBZ	X-Ray	2.30 Å
HHDBT	1P84	X-Ray	2.50 Å

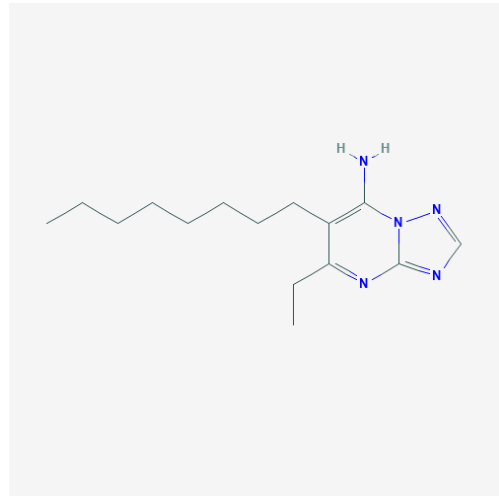
Table 3: Crystal structures of the Yeast bc1-complexe with inhibitors

Furthermore, the following inhibitors could be found in a literature research Oudemansin²⁵, Funiculosin²⁶, Ametoctradin^{27,28}, Pyrimoprph, ELQ271²⁹, Picoxystrobin, Pyraclostrobin, Cyazofamid²⁸, Amisulbrom²⁸, Hydramethylnon, Pyrimorph.

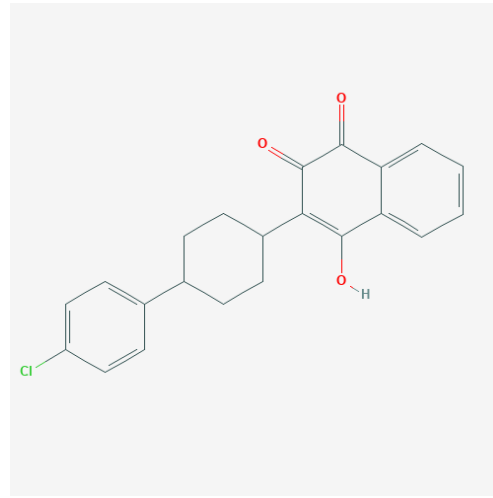
The structures of the 30 used inhibitors for the docking experiments and virtual screening are displayed in Table 4, for each binding side.

Qo-site

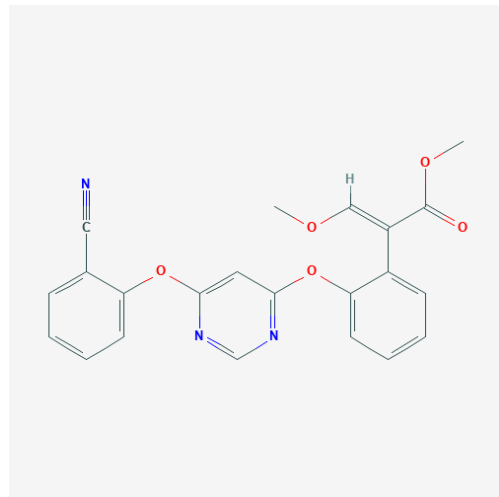
Ametoctradin



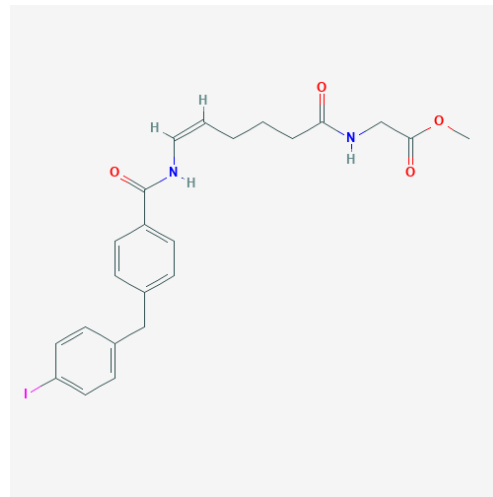
Atovaquone



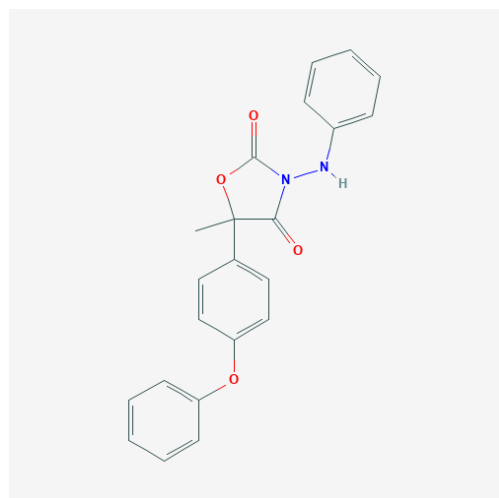
Azoxystrobin



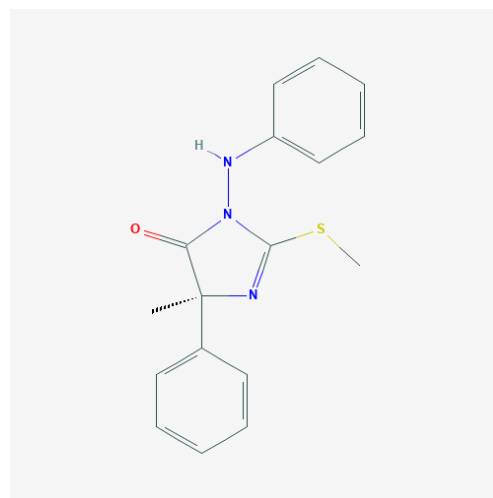
Crocacine-Iod



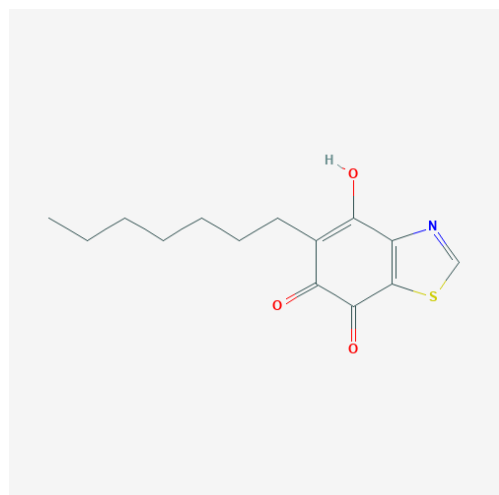
Famoxadone



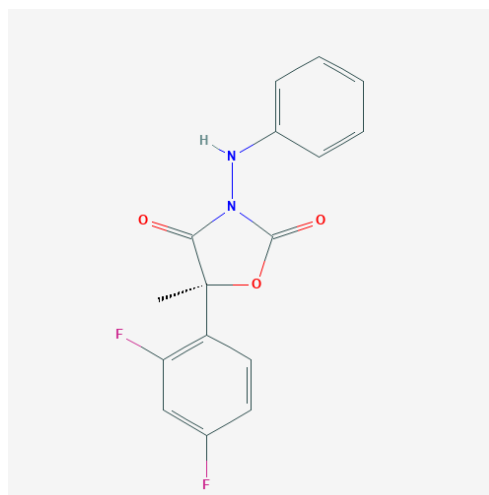
Fenamidon



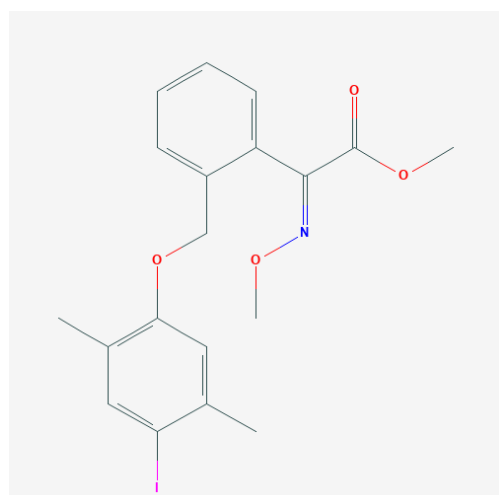
HHDBT



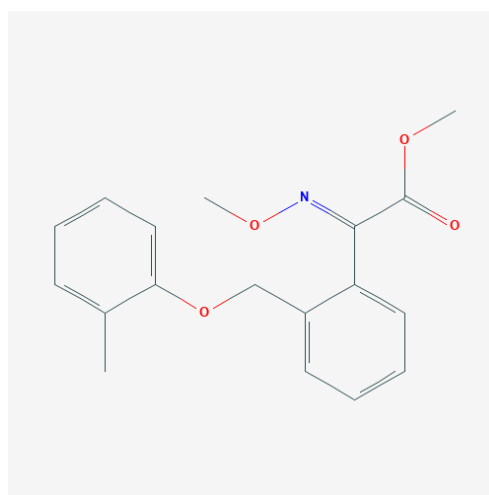
JG144



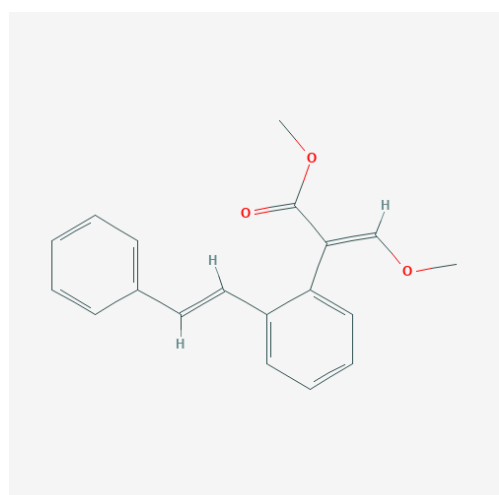
Kresoxim-l-dimethyl



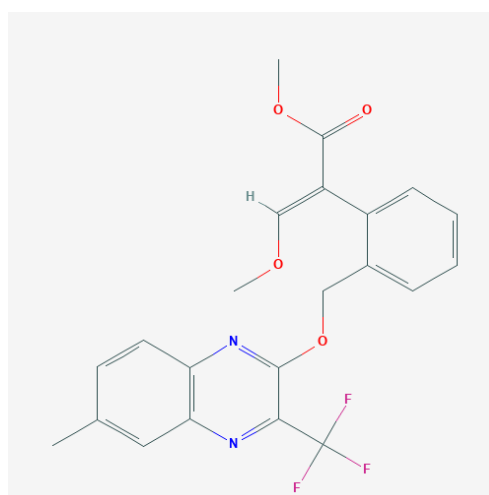
Kresoxim-methyl



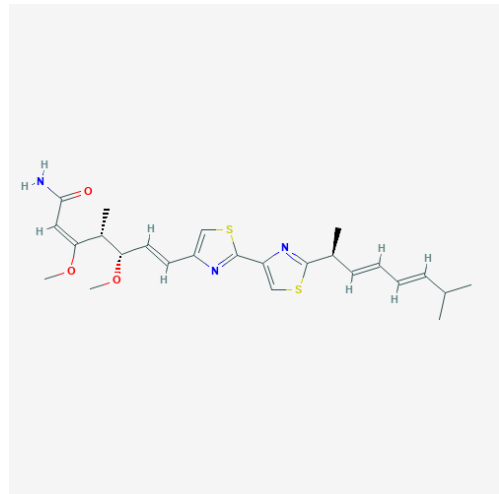
MOA (Methoxy-acrylate-stilbene)



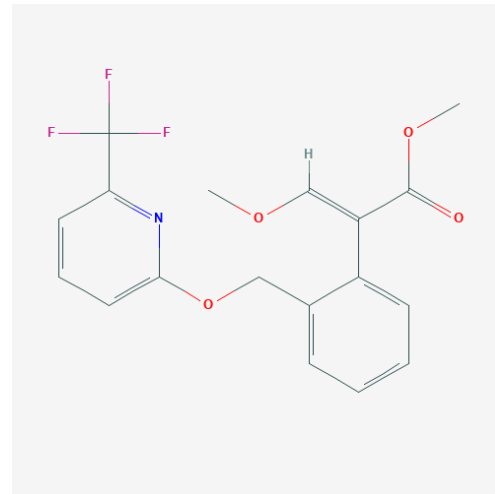
MOA-F



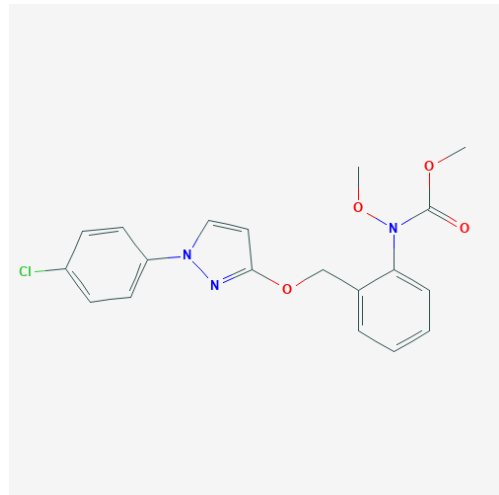
Myxothiazole



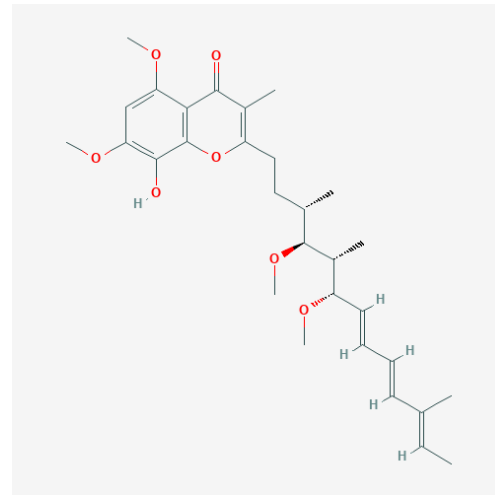
Picoxystrobin



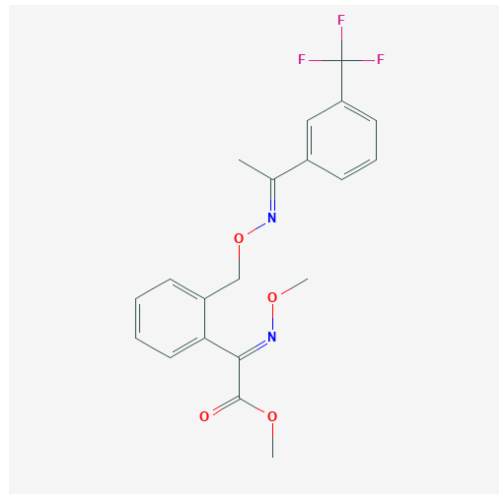
Pyraclostrobin



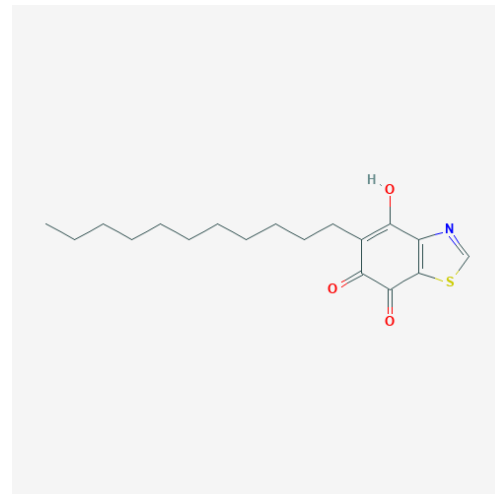
Stigmatellin A



Trifloxystrobin

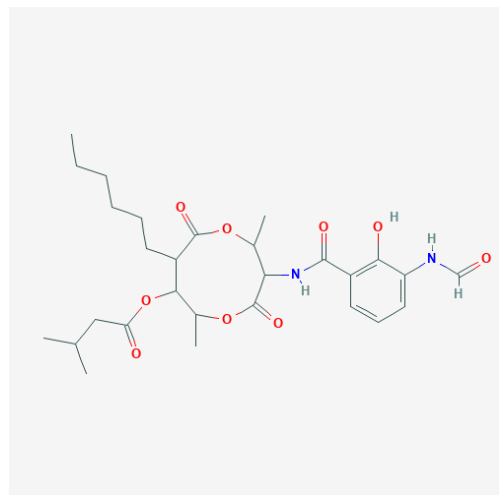


UHDBT

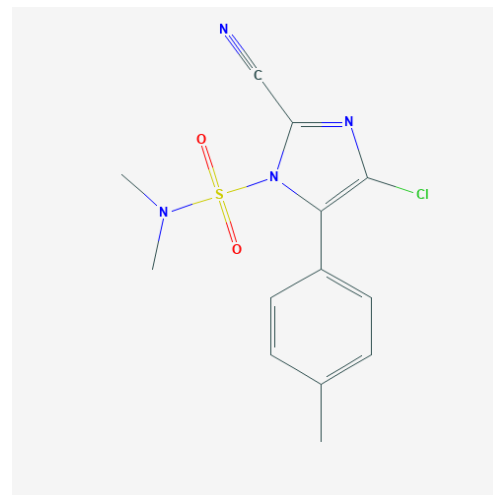


Qi-site

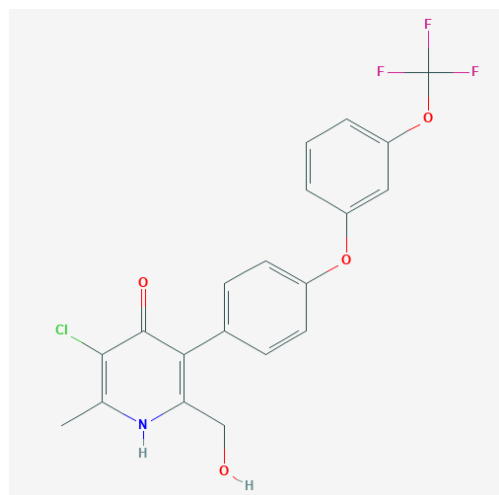
Antimycin



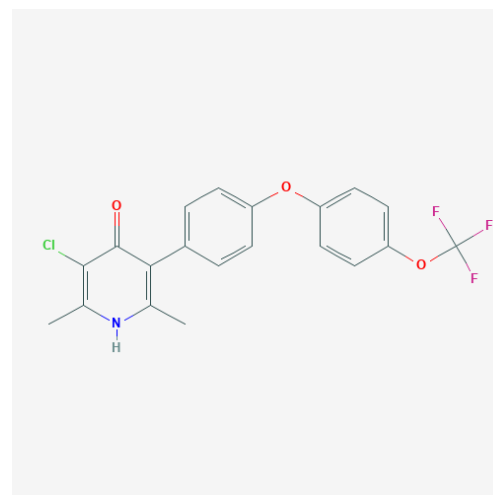
A₁ Cyazofamid



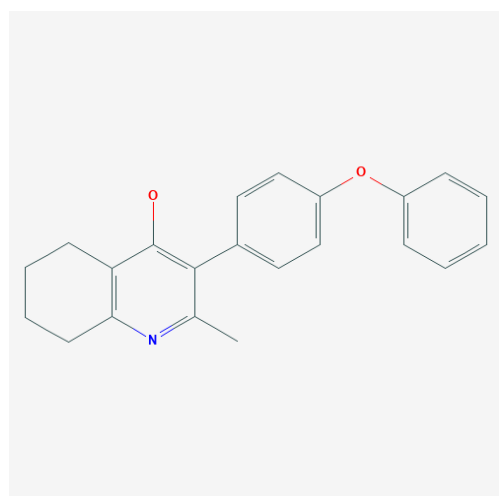
GSK932121



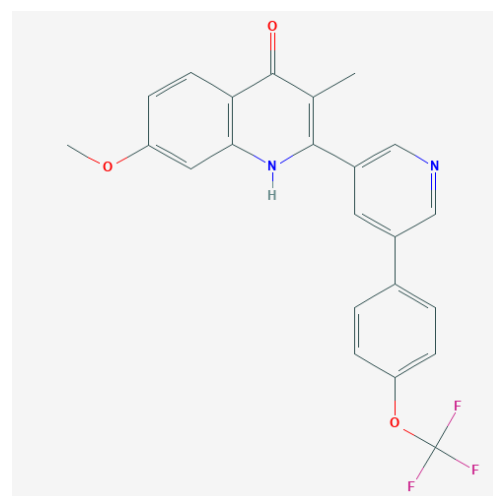
GW844520



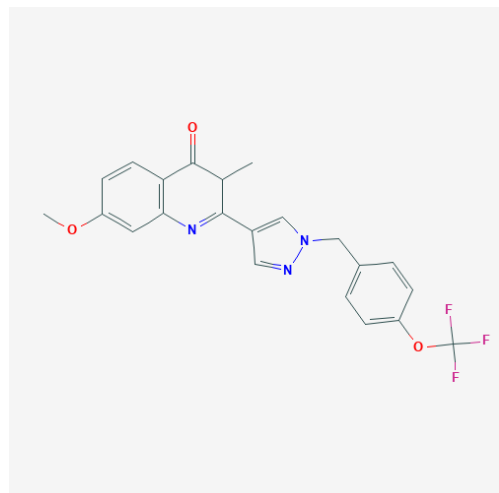
MJM150



SCR0911

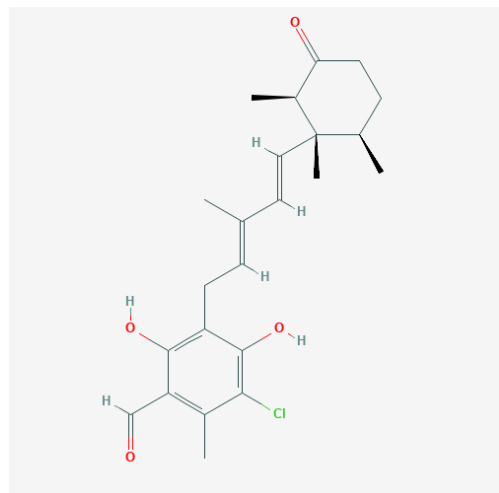


WDH2G7

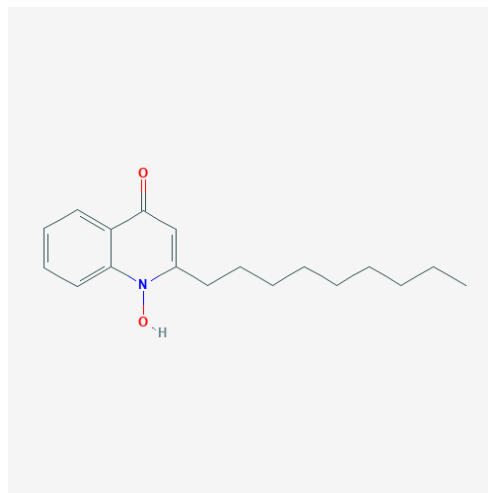


Qo + Qi site

Ascochlorin

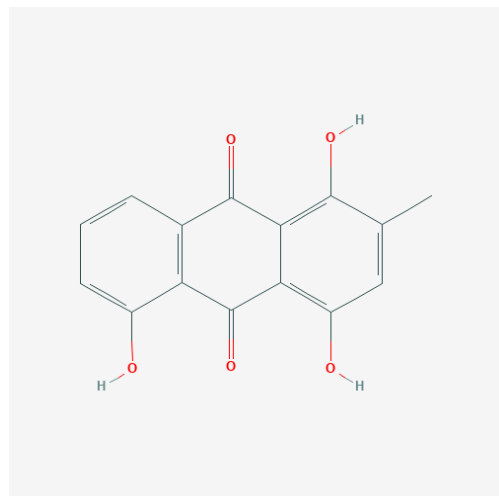


NQNO

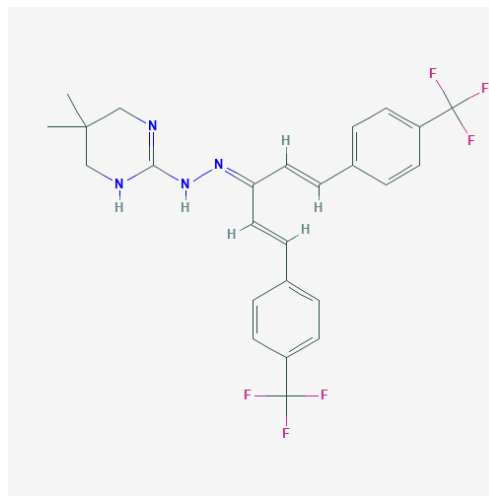


unkown binding site

Funiculosin



Hydramethylnon



Pyrimorph

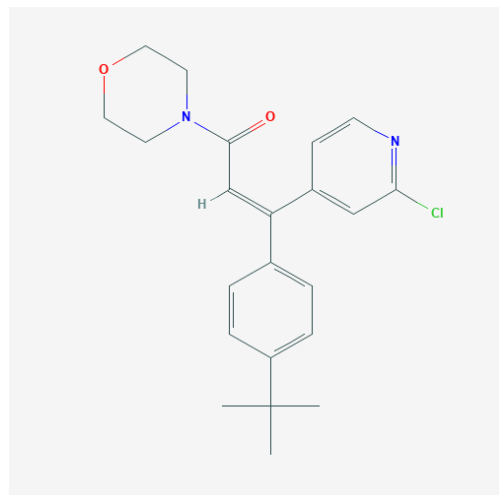


Table 4: Structures of the 30 inhibitors

5.1.2 Promals 3D

Promals 3D is an online tool to align several protein sequences and structures.³⁰ It was used for comparing the various species *Bos taurus*, *Gallus gallus*, *Sacharomyces cerevisiae* und *Rhodobacter sphaeroides* with the human sequence. (Table 5)

5.1.3 Uniprot

Universal Protein Resource is an online science database that provides protein sequence and functional information. The three institutes European Bioinformatics Institute (EMBL-EBI), Swiss Institute of Bioinformatics (SIB) and Protein Information Resource (PIR) have been working in cooperation on the database since 2002.³¹

5.1.4 Drugbank

Drugbank, a free available databank, grant access to bioinformatic and chemical information on drugs and their target structures. The first version 1.0 of Drugbank was published in 2006 and has been expanded over the years. The database, 2021 latest released Version 5.1.8, contains 14.583 drug entries including 2.701 approved small molecules drugs, 1.499 approved biologics (proteins, peptides, vaccines and allergenics, 132 neutraceuticals and over 6.653 experimental drugs (discovery-phase).^{32,33} This platform makes it easier for natural scientists such as chemists, pharmacologists or pharmacists to access relevant data for their work and research.³³

5.2 Docking Studies

Molecular docking is indispensable these days. The computer-aided research, as already mentioned at the beginning, is of great importance and enables predictions in the protein-ligand interaction. In the algorithms, interactions such as Coulombic interactions, Van der Waals forces or hydrogen bonds are included in order to be able to calculate the bonding possibilities. Lead compounds can be found and optimized using the docking strategies.³⁴

Over the years, the view of a rigid system of protein-ligand binding has further developed. The so-called “key and lock” principle, first described by Emil Fischer in 1894, was replaced by the “induced-fit” model. Ligands and their target protein cannot be seen as a rigid system, there is always a certain amount of movement and flexibility possible.

There are several programs with different search algorithms and scoring functions for docking, each application has its own advantages and disadvantages.

This thesis mainly performed with Glide and Induced-fit docking from Schrödinger in Maestro. Some docking studies with Gold were also tried.

5.2.1 Software

5.2.1.1 Maestro (Schrödinger)

Schrödinger is one of the most popular program developers for docking experiments and virtual screening.

Some applications from Schrödinger, such as “LigPrep” and “Glide”, are operated via the Maestro graphical user interface. It is used to visualize structures that, as in our case, can be imported using a PDB file.³⁵

Schrödinger's application uses the “Protein Preparation Wizard” to provide the protein preparation. This is necessary to ensure chemical correctness and to optimize the structures for use with Glide. The crystal structures are only reconstructed by electron density. Incorrect side chains can occur in the PDB structures and have to be corrected. Schrödinger also offers ligand preparation using “Ligprep”. Therefore, several processing steps are carried out in order to optimize the structures, for example the protonation state or tautomeric are important.

Glide

Glide (Grid-based Ligand Docking with Energetics) is a docking program that uses algorithms for conformation generation, torsion optimization and energy minimization. Ligand poses are generated and rated, which are ultimately ranked by scoring.

You can choose between three docking precision modes, HTVS (high-throughput virtual screening), SP (standard precision) and XP (extra precision). The first method is the fastest, but also a very limited screening. The most powerful is the XP mode, but it takes more time to calculate.

At the end, poses are generated along with a number of properties, such as scoring function, ligand efficiency metrics and various indices to discriminate ligands with similar docking score values.

Induced-Fit Docking

A rigid receptor model is assumed for glide docking. Some movement of the receptor or ligand is taken into account, but in some cases this may not be sufficient. If a ligand binding contributes to the conformation change, the whole system must be assessed more flexibly. For this purpose, it combines the Glide and Prime Refinement, which allows the receptor in the binding site to better adapt to the shape of the ligand.³⁶

5.2.1.2 GOLD

GOLD (Genetic Optimization for Ligand Docking) is a genetic algorithm for docking flexible ligands into protein binding sites. The program is well established for docking experiments and achieves reliably pose prediction performance and good results in virtual screening.^{37,38}

5.2.1.3 Visualization programs

MOE

Molecular operating environment, is a program for scientific research. It can be used for Ligand-based or Structure-based drug design, Docking studies and Virtual Screening. For this thesis it was used for visualizing the crystal structure in order to decide which residues should be flexible for the docking in GOLD.

Pymol (Schrödinger)

It is another application to visualize 3D structures, which was also used for comparison of the binding sites and check the interactions with the ligands.

5.3 Pharmacophore modeling

The interactions of a ligand with the target are defined by physicochemical interactions such as hydrogen bonds, dipole/dipole interactions, ionic interactions, and hydrophobic interactions. Their arrangement in the 3D-space are called pharmacophore. The pharmacophore modeling and virtual screening of databases helps to identify new hit structures.

5.3.1 Software

LigandScout is a program to create structure- and ligand-based pharmacophore models. It works with algorithms for performing alignments and interpreting and

customizing ligand-macromolecule interactions. The program automatically creates pharmacophore models after loading PDB files, which you can edit and refine. It contains in-silico screening of compound libraries, and tools for analyzing the performance of the models.³⁹

Version 4.4 was used for the pharmacophore modelling of both binding sites.

5.4 Knime Workflow

Knime, an open source software, is an analytic platform for creating data science workflows. You can easily construct workflows to link, filter and visualize large amounts of data. The tasks are represented as nodes, this enables data to be read, written, transformed and models to be created and visualized. Many workflows, nodes and components are provided by the Knime hub so they can be downloaded and used easily.

5.4.1 Pareto Ranking

Data are ranked without improving one property and without having to worsen another at the same time. The results from the docking experiments and the pharmacophore screening could be combined and subsequently analysed by machine learning. The ranking was carried out by pharmacophore fit-score and docking-score.

The pharmacophore fit-score is calculated by the number of matching pharmacophore features and the RMSD of the pharmacophore alignment.³⁹

6 Results and Discussion

The first step during the literature research was a summary of the existing PDBs and inhibitors, which are listed in Table 1 and Table 2.

Many crystal structures (PDB: 1L0L, 1NTK, 1NU1, 1PP9, 1PPJ, 1SQB, 1SQP, 1SQQ, 1SQV, 1SQX, 2A06, 2BCC, 2FYU, 2IBZ, 3BCC, 3CWB, 3H1J, 3HLI, 3L70, 3L71, 3L72, 3L74, 4L75, 3TGU, 4D6T, 4D6U, 5KLV, 5NMI, 5OKD, 5XTE, 6FO0, 6FO6 and 6HAW) have been aligned with the PDBeFold webserver to be able to compare them visually. This step was necessary because different programs and their algorithms generate different coordinates.

We compared the amino acid sequences of four species with PROMALS 3D, which are shown in Table 5. For the alignment you have to enter the protein sequences in FASTA format (available from UniProt), the protein structure with the PDB, and the selected chain of the binding pocket.

Homo sapiens:

5XTE → Cyt B → Chain J+V → UniProtKB P00156 (CYB_HUMAN)

Bos Taurus :

1SQB → Cyt B → Chain C → UniProtKB : P00157 (CYB_BOVIN)

Gallus gallus :

3L71 → Cyt B → Chain C+P → UniProtKB : P18946 (CYB_CHICK)

Rhodobacter sphaeroides :

6NHH → Cyt B → Chain A+E → UniProtKB Q02761 (CYB_RHOSH)

Saccharomyces cerevisiae :

2IBZ → Cyt B → Chain C → UniProtKB : P00163 (CYB_YEAST)

Colored PROMALS3D alignment (sequences in aligned order)

Table with 3 columns: Species/Chain ID, Sequence, and Position. It shows multiple alignments for different species (e.g., 6nhh, 1sqb, 3171, 5xte) and chain types (CYTOSOL, BOVINE, CHICK, HUMAN). Consensus sequences are provided at the bottom of each alignment block.

Table 5: Sequences of the bc1-complex from the various species

It shows a high sequence identity between the species, especially in the bovine, chicken, and human complex. The high conserved residues are indicated by symbols in Table 1.

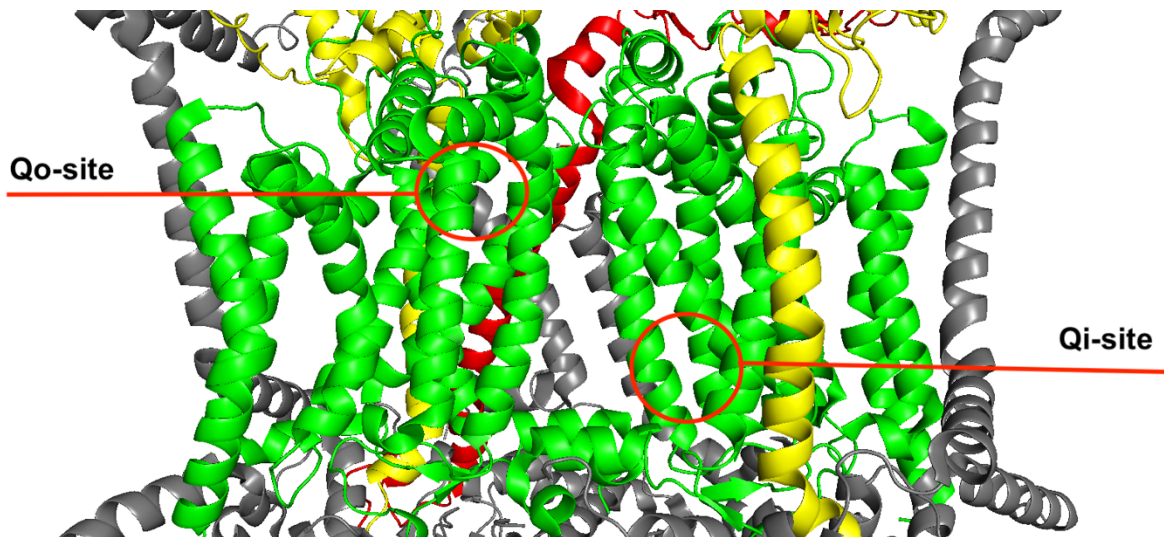


Figure 6: human complex with both binding sides

A meaningful interaction of the Qo-site takes place in the PEWY-sequence, there is usually a hydrogen bond to Glu271. Many of the Class P inhibitors form this important hydrogen bond, like the inhibitor stigmatellin in the figure below ^{7,14}

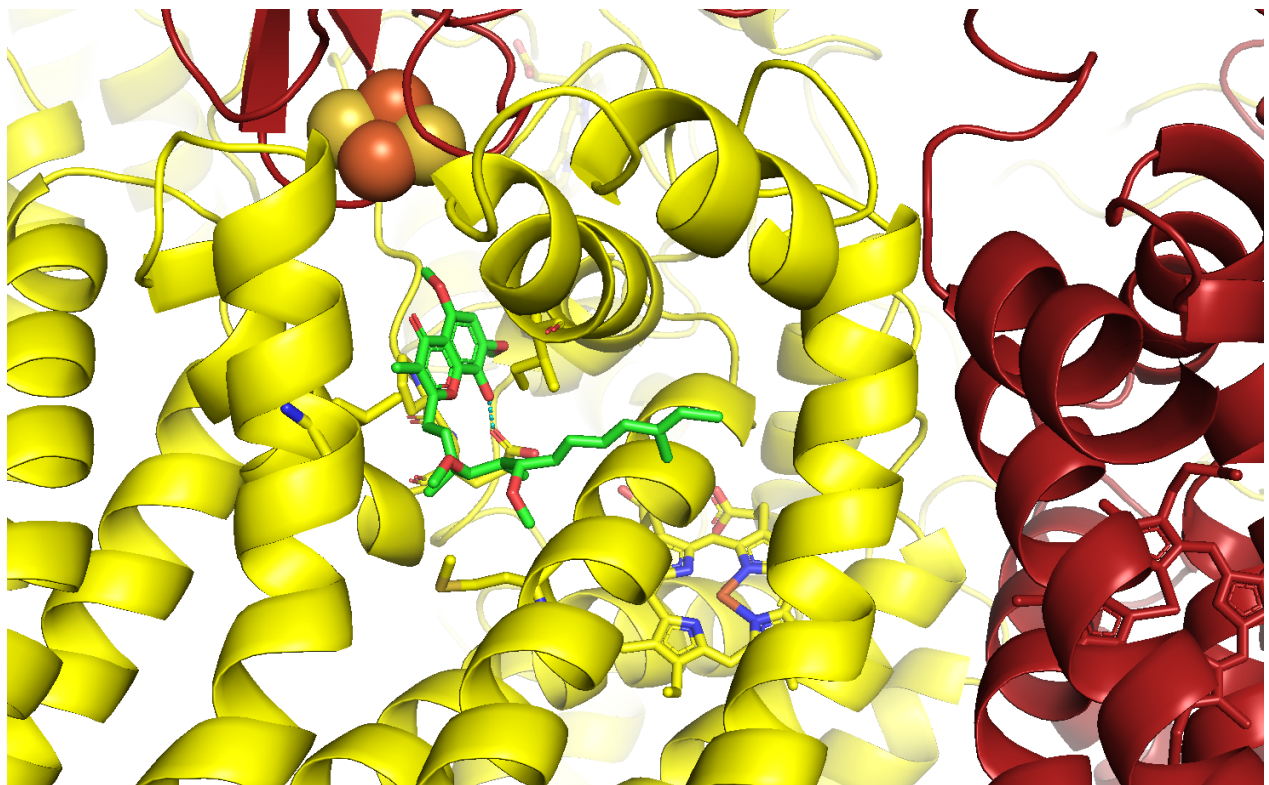


Figure 7: PDB 1SQX with the co-crystallized inhibitor Stigmatellin and the h-bond to Glu271

The residues Ile146 of the cd1 helix and Pro270 and Glu271 from the PEWY sequence form a narrow constriction in the binding pocket, where planar substrates or inhibitor head groups can insert.⁷

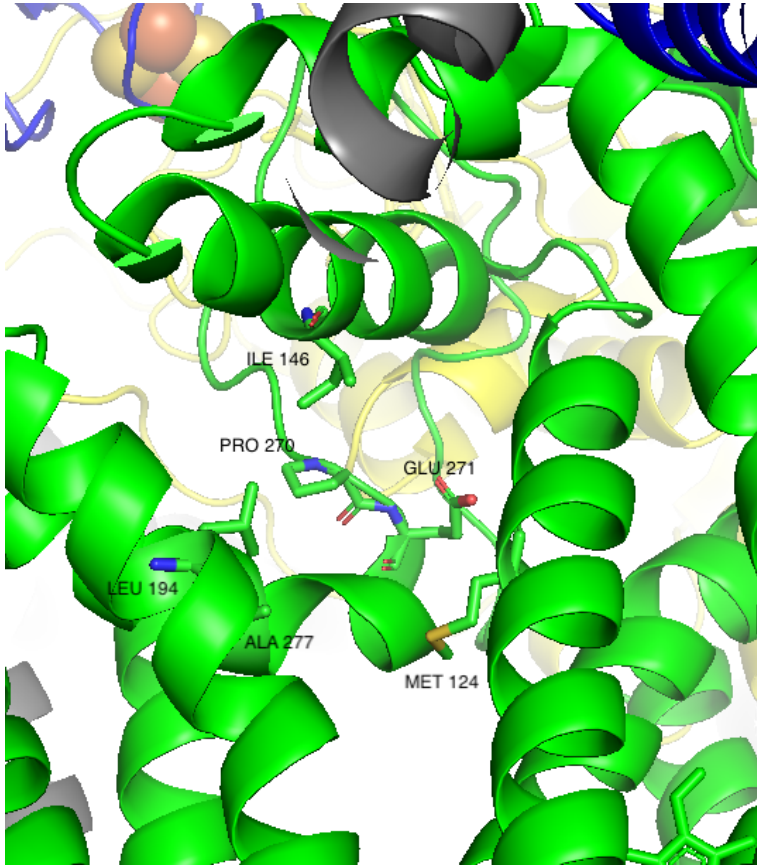


Figure 8: Qo-binding side of the human complex and the most important side chains are labeled

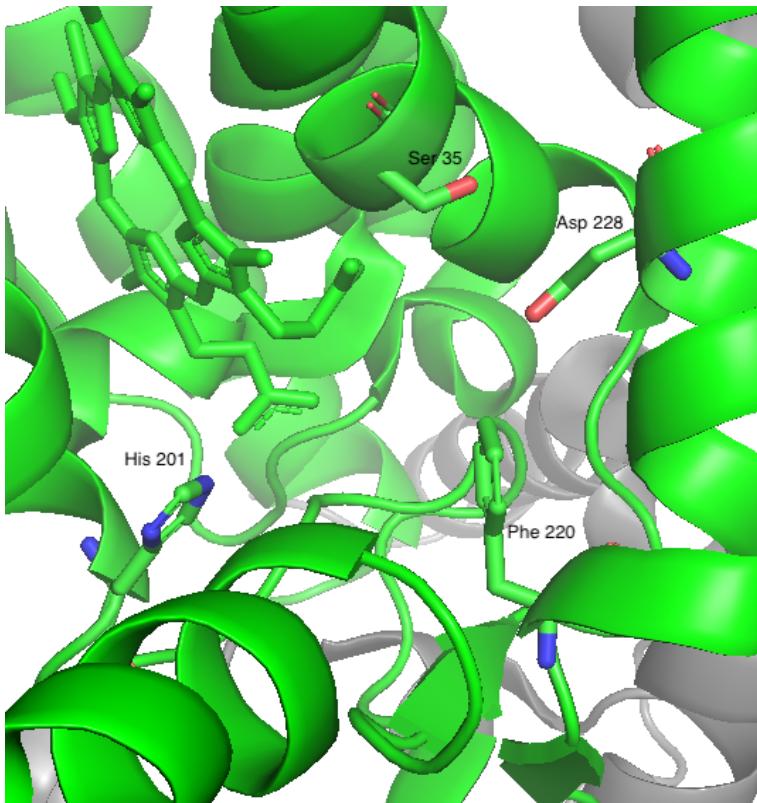


Figure 9: Qi-binding side of the human complex with the most important residues

Qo-site	Qi-site
Glutamic acid /Glutamate 271	Aspartic acid/ Aspartate 228
Tyrosine 273	Serin 35
Methionine 124	Histidine 201
Phenylalanine 128, 274	Lysine 227
Isoleucine 146	Tryptophane 31
Proline 270	Phenylalanine 220
Alanine 277	Proline 24
Leucine 294	Isoleucine 39, 42
Valine 145	Leucine 200

Table 6: Comparison of the two binding sites of the most important amino acids

There are many hydrophobe, aromatic-aromatic and π -interactions in both binding sides.

A study²⁷ describes a sequence identity of the bovine cyt. b (1PPJ) of 50.92% with yeast (3CX5), 74,67% with chicken (1BCC) and 49,08% with Rhodobacter capsulates. The identity analysis of the amino acid sequences of bovine, chicken and human was also investigated in MOE to prove the similarity of their binding pockets. It matched in a range of 72.4 – 78,8%. (Figure 10 and Figure 11)

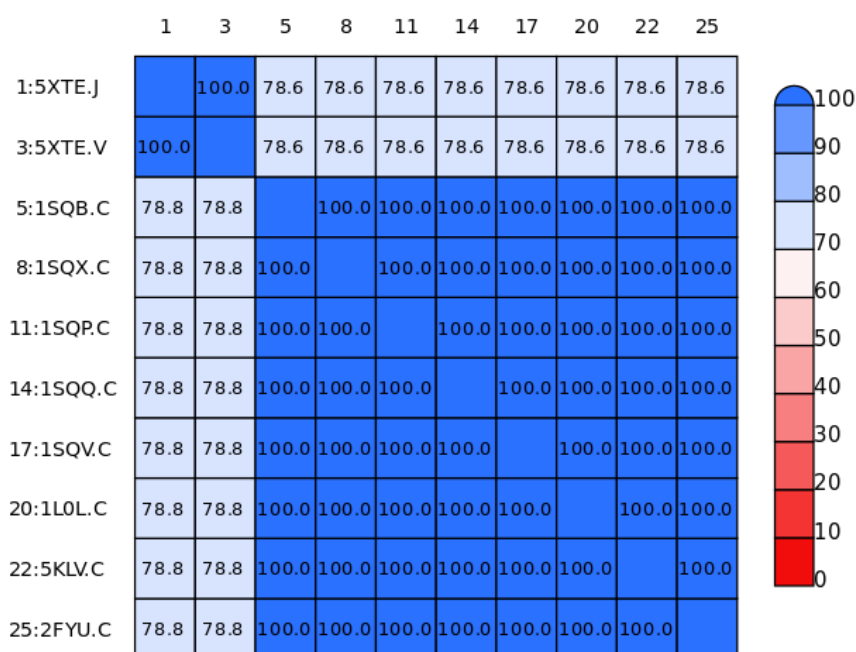


Figure 10: Comparison of the PDBs identity between cyt. b of bovine and human complex

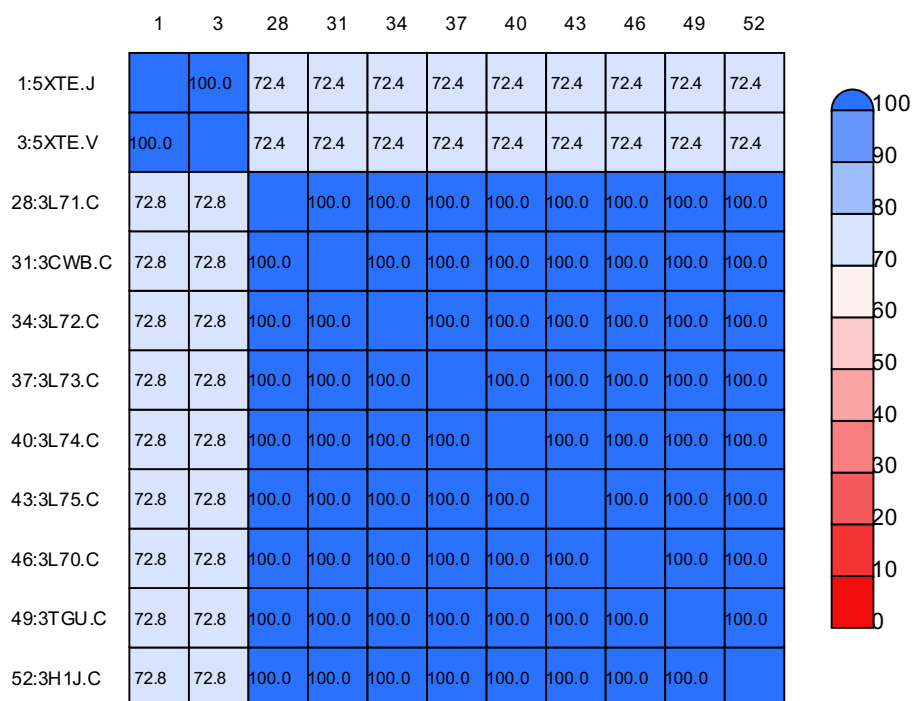


Figure 11: Comparison of the PDBs identity between cyt. b of chicken and human complex

6.1 Docking

6.1.1 Glide Docking Experiments

The first step was to simulate the reproducibility of the inhibitors in their crystal structures by redocking in Maestro 19-3.

The following PDBs, in Table 7 and Table 8, were selected for the redocking experiments.

PDB	Inhibitor
1SQP	Myxothiazole
1SQQ	MOAS
1SQX	Stigmatellin
1SQV	UHDBT
3L72	Kresoxim-l-methyl
3L70	Trifloxystrobin
1SQB 3L71	Azoxystrobin
3H1L	Ascochlorin

Table 7: used PDBs for the Qo-Site Redocking

PDB	Inhibitor
1NTK	Antimycin
5NMI	MJM
1NU1	NQNO
3H1L	Ascochlorin
5OKD	SCR0911

Table 8: used PDBs for the Qi-Site Redocking

The protein preparation was prepared with the “protein wizard panel” using the default settings. Ligand preparation was done with die LigPrep panel. The Glide Grid was generated centroid of the ligand and the XP mode was selected.

As far as the docking was successfully reproducible, this was checked visually by demonstrating the most important interactions or with their overlaid PDB compared, which are enumerated in Table 1.

There were reproducibility problems only with Azoxystrobin. Either there were no outputs after the docking try or the ligand was always flipped in the binding pocket and therefore cannot establish the essential interactions.

Because of these issues, we tried it with the other docking program GOLD. For this purpose, as mentioned at the beginning, the positions of the amino acid side chains of the various ligands were analyzed, since with GOLD the side chains have to be selected manually for a certain flexibility.

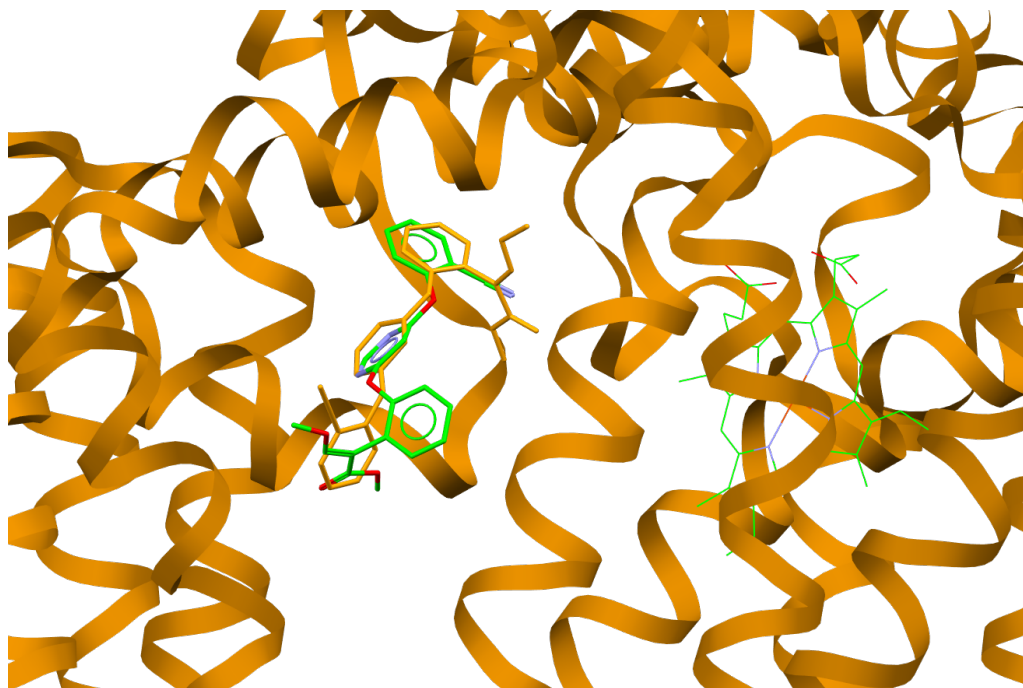


Figure 12: Docking Result of Azoxystrobin (green from docking, orange from PDB) in GOLD

Unfortunately, the results were the same as with Maestro, always in a flipped position. (Figure 12)

Stigmatellin could be reproduced with GOLD.

Docking Experiments with drugbank

Further docking runs were carried out by screening drugbank to find drugs that inhibit CIII. The PDB of the inhibitors antimycin A (1PPJ), myxothiazole (1SQP) and stigmatellin A (1SQX) were selected because they represent the three different classes of inhibitors. The protein preparation was performed in maestro 19-3 using the Protein Preparation Wizard. The center of the grid was the centroid on the respective inhibitor, the SP mode was used with the standard settings, and one pose per ligand was generated in the output.

The following known inhibitors were found among the results of the docking experiments. Unfortunately, no antimycin was found with 1PPJ, but famoxadone (docking score: -7.178), myxothiazole (d.s. : -5.176) and azoxystrobin (d.s. : -4.21). With the PDB 1SQX myxothiazole (d. s.: -12.25), and famoxadone (d.s.: (-9.318.) were found. With the third PDB 1SQX, famoxadone (d.s. : -8.909) and myxothiazole (d.s.: -8.393) were also found.

The results, especially the docking scores, were used for the evaluation with the pharmacophore modelling in a Knime workflow, which will be explained later.

Docking Experiments with 30 Inhibitors

The PDB of the inhibitors antimycin A (1PPJ), myxothiazole (1SQP) and stigmatellin A (1SQX) were selected because they represent the three different classes of inhibitors. The ligand preparation of the 30 inhibitors was performed in maestro 19-3 using Ligprep. The other settings were the same as for the previous docking experiment with drugbank.

The scores were also included in the evaluation at the end for the machine learning.

6.1.2 Induced-fit Docking Experiments

Maestro 19-3

We wanted to show the similarity between the species and docked six of the inhibitors into the Qo-site of the human complex. We decided for induced-fit docking, because this method allows a better flexibility and adaptation of the protein-ligand interaction during the docking process. There is only the nature crystal structure available of the human complex (PDB: 5XTE).

First, the human complex was reduced so that the work process was shortened. The larger the protein, the longer the induced fit docking runs. The protein preparation of 5XTE was performed after the chain reduction in Maestro with the protein wizard panel. The chains K, O, W, X, Y were deleted to make the protein smaller.

Since there are no bound ligands in the human crystal structure, the side chains had to be determined in order to generate the grid for the docking.

The selected residues were Phe128, Ile146, Pro270, Glu271, Ala277, Leu294, Met124. At the beginning only 8 inhibitors were docked, stigmatellin, MOA, trifloxystrobin, famoxadone, fenamidone, JG144, myxothiazole, and NQNO.

The first docking try was performed with the complex's V-chain, but the process was aborted after a short time. Then the next docking experiment was attempted in the J-chain of the bc1-complex, which was successful.

It was a mystery why it didn't work in this chain because the sequence should be equal to the dimeric J-chain. Unfortunately, we could not find out why it is not possible to dock in the V-chain of the human complex.

Regrettably, the results were not satisfactory because the ligands were docked too far outside and could not enter the essential interactions with the binding pocket.

We tried the next docking experiment with an artificial membrane because the binding site is very close to the outside of the membrane. Perhaps the calculations of the algorithms would give different docking results and stigmatellin would also form the desired hydrogen bond.

We also no longer used all of the previously selected side chains, but focused the glide grid on 128, 270, 271, 146. Thus, the remaining residues 124, 294, and 277 were left out, as they are perhaps too far outside of the binding pocket.

The results were successful for the best-scored ligands so far, because the important hydrogen bond to Glu271 could be demonstrated with MOA, trifloxystrobin, famoxadone, fenamidone, myxothiazole and JG144.

Only stigmatellin was again a little too far outside the binding pocket so that no interaction with Glu271 could be established. This could possibly be due to the lack of water in the binding site. In the case of bovine crystal structures, there is a water atom in the binding pocket that could possibly help stabilize the ligand binding.

A hydrogen bond to Glu271 was also formed to NQNO. This cannot be visually compared with the crystal structure of the bovine complex, since in its PDB only the Qi-site NQNO is shown. The hydrogen bond from NQNO to Glu271 was described in a study, so the interaction was evaluated positive and reproduced.¹¹

GOLD

First, the PDBs had to be compared with the human complex in order to determine which side chains had to be selected flexibly. In GOLD it is indicated manually which residues should be movable.

The first docking experiment was determined with the coordinates X: 9.6771, Y: 132.3063, Z: 80.9657 of the Qo-site, a selected point to define a center in the binding pocket. You can choose 10 flexible side chains, these were Met124, Phe128, Tyr131, Met130, Ile146, Glu271, Tyr273, Phe274, Leu275, Leu294. The following ligands were docked Azoxystrobin, Famoxadone, Fenamidone, JG144, MOA, Myxothiazole, Stigmatellin and UHDBT.

For the second docking experiment the coordinates X: 8.8592, Y: 128.5908, Z: 824553 were defined, a selected point to define a center in the binding pocket.

The last docking attempt has the coordinates X: 7.77264, Y: 132.2520, Z: 80.8911, a comparison of the ligands from the aligned bovine complex to set a point in the binding pocket.

The results of all three dockings were unsuccessful because the desired interactions could not be established. The docked inhibitors are always too far outside and not inserted in the middle of the pocket.

6.2 Pharmacophore modeling

The preparation of the pharmacophores was a challenge, as the inhibitors have quite different structures and interactions, especially in the hydrophobic outer part of the pocket. Due to the three classes of inhibitors, it was not possible to create one pharmacophore scaffold, and therefore two pharmacophores were generated for each binding pocket.

6.2.1 Qo-Site

The following PDBs were used for this binding site to create two pharmacophores of the different binding modes.

For the first pharmacophore (Figure 13) with the inhibitor Myxothiazole (1SQP), a hydrogen bond acceptor to the nitrogen of Glu271 (red vector), two fixed and one optional hydrophobic interaction (yellow spheres) were created.

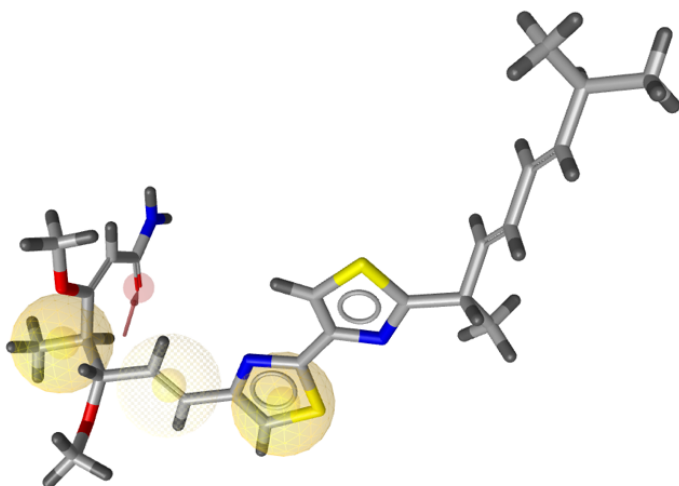


Figure 13 Qo-site pharmacophore 1

The second pharmacophore (Figure 14) was generated with the PDB 1SQX, bound with Stigmatellin, with one hydrogen bond donor to the oxygen of Glu271 (green sphere) and two hydrophobic areas (yellow spheres).

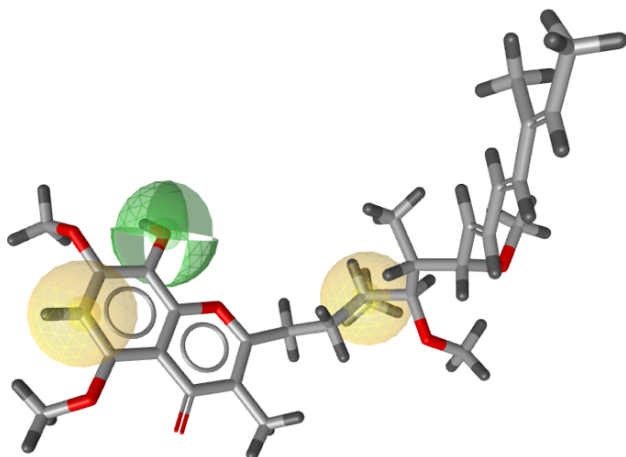


Figure 14 Qo-site pharmacophore 2

These two pharmacophores were finally combined for the Qo-binding site during the screening.

6.2.2 Qi-Site

For the second binding pocket, two pharmacophores were created with the PDB 1PPJ of the inhibitor Antimycin. The other ligands were also included for this Site in order to determine the hydrophobic properties, which are more on the outside of the pocket and differ more between some inhibitors. We overlaid the ligands to decide where we should set the hydrophobic areas (number 1 + 2 spheres in Figure 15) Figure 15 Qi-site both pharmacophores. The pharmacophores contain one fixed (red sphere) and one optional (red dotted sphere) hydrogen acceptor, a hydrogen donor and three hydrophobic interactions, two of them are arranged differently in the models. The first pharmacophore is with the number one of the hydrophobic areas and the second is with number two, as you see below. (Figure 15)

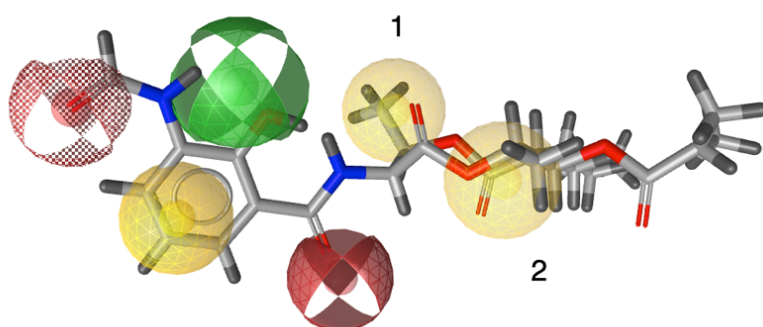


Figure 15 Qi-site both pharmacophores

The pharmacophores for both binding sides were evaluated with a screening of the 30 inhibitors library, which was created beforehand.

During the screening of the self generated ligands library, the following 12 hits were found for the Qo site with the two pharmacophores 1 or 2: Azoxystrobin, Fenamidone, MOA, Kresoxim-I-dimethyl, Kresoxim-I-methyl, Ametoctradin, JG144, Myxothiazole, Picoxystrobulin, Crocacin Iodine, NQNO and Stigmatellin.

In the case of the other binding pocket, the control with the 30 inhibitors library retrieved 6 hits: Antimycin_A, Aschochlorin, Funiculosin, GSK932121, GW844520, NQNO.

For further analysis, the “pharmacophore fit score” function was used in Knime.

6.3 Knime Workflow

In order to be able to combine the data collected from the docking experiments and the pharmacophore models, a workflow was created in Knime.

Docking experiments of drugbank with 1PPJ, 1SQX and 1SQP were combined with pharmacophore screening of drugbank in order to link the structure-based scores.

For the evaluation, the docking experiment was carried out with the 30 inhibitors in the PDB 1PPj, SQX and 1SQP and this hit list was also linked with the pharmacophore screening of the 30 inhibitors.

Finally, the docking experiments with the pharmacophore screening of drugbank and the docking experiment with the pharmacophore screening of the 30 inhibitors were linked and evaluated by Pareto ranking, which includes the structure-based docking score and pharmacophore fit-score.

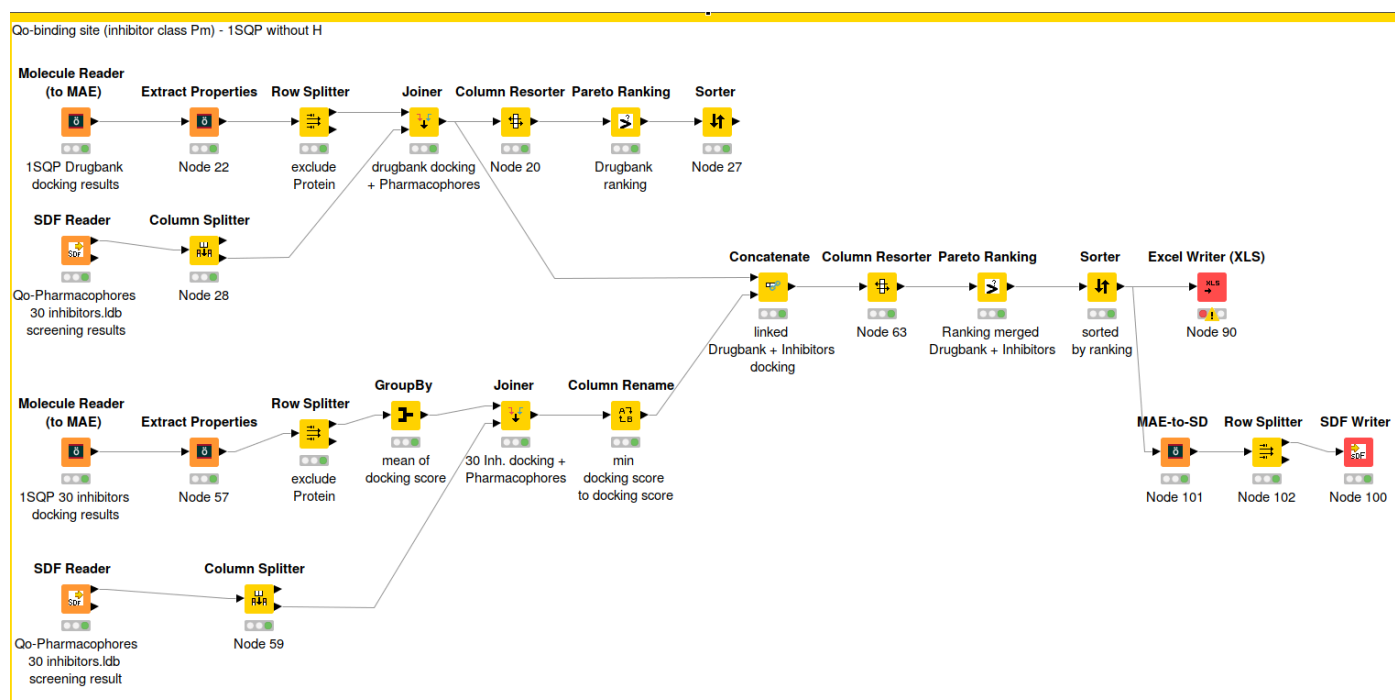
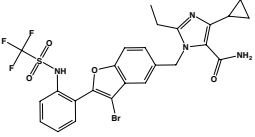
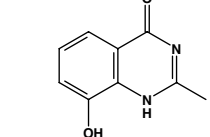
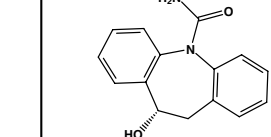
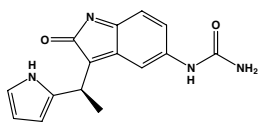
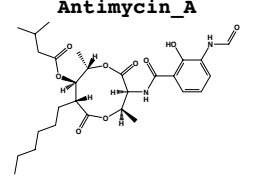
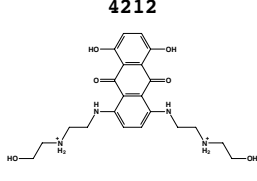
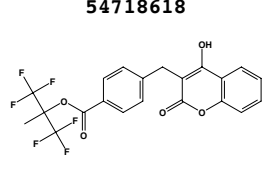
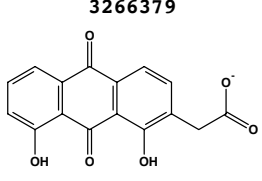
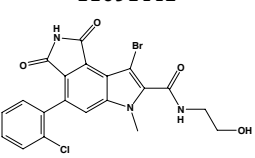
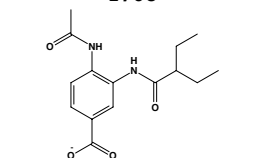
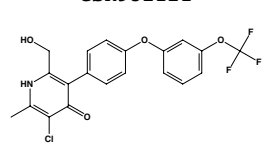
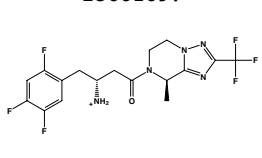
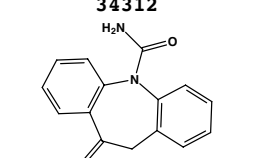
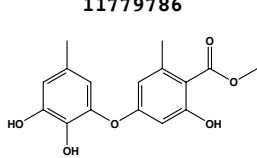
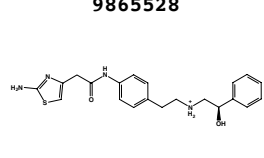
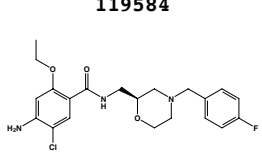
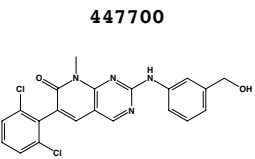
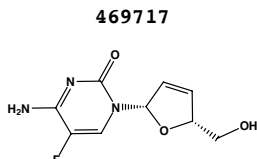
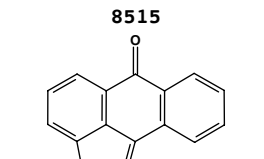
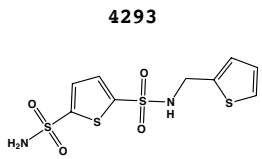


Figure 16: Knime workflow for the Qo binding site with the PDB of 1SQP

Among the top 20 of the Pareto ranking in the 1PPJ PDB, antimycin was listed in rank 1 and GSK932121 in rank 2 of the 30 inhibitors. This can be rated as a successful control, as they were ranked high as known inhibitors.

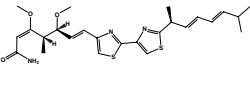
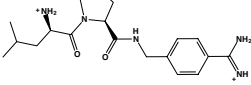
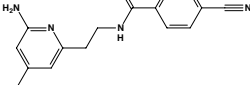
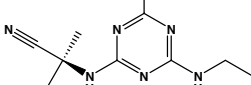
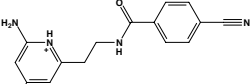
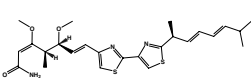
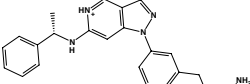
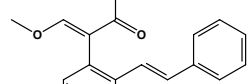

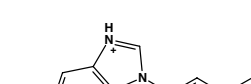
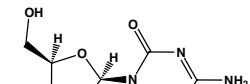
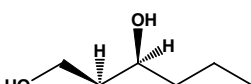
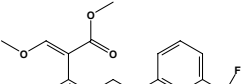
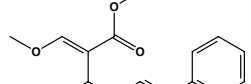
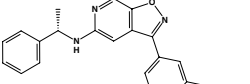
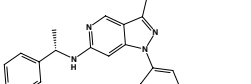
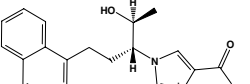
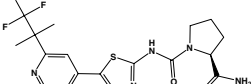
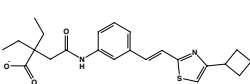
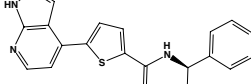
<p>60921</p>  <p>Pareto Rank: 1 DB01347 Sapisartan 46.0700 -7.8666</p>	<p>63306</p>  <p>Pareto Rank: 1 DB02690 NU1025 46.9700 -7.8457</p>	<p>9881504</p>  <p>Pareto Rank: 1 DB14575 Eslicarbazep 47.7400 -7.1990</p>	<p>46937053</p>  <p>Pareto Rank: 1 DB07132 1-(2-Oxo-3-[56.3400 -6.8221</p>
<p>Antimycin_A</p>  <p>Pareto Rank: 1 56.6900 -6.8190</p>	<p>4212</p>  <p>Pareto Rank: 2 DB01204 Mitoxantrone 45.8400 -7.5587</p>	<p>54718618</p>  <p>Pareto Rank: 2 DB12823 Tecarfarin 46.9600 -7.3575</p>	<p>3266379</p>  <p>Pareto Rank: 2 DB03037 Oxidized Ace 56.1200 -6.5815</p>
<p>11691442</p>  <p>Pareto Rank: 2 DB08365 8-bromo-4-(2- 56.1400 -6.1522</p>	<p>1708</p>  <p>Pareto Rank: 2 DB07762 4-(N-ACETYLA 56.2700 -5.5830</p>	<p>GSK932121</p>  <p>Pareto Rank: 2 46.8500 -7.5203</p>	<p>23661697</p>  <p>Pareto Rank: 3 DB07081 (2R)-4-[(8R) 46.7800 -7.3531</p>
<p>34312</p>  <p>Pareto Rank: 3 DB08776 Oxcarbazepin 47.4300 -6.5548</p>	<p>11779786</p>  <p>Pareto Rank: 3 DB08179 methyl 4-(2, 55.8700 -6.3653</p>	<p>9865528</p>  <p>Pareto Rank: 4 DB08893 Mirabegron 45.2700 -7.2368</p>	<p>119584</p>  <p>Pareto Rank: 4 DB11675 Mosapride 46.4700 -7.0512</p>
<p>447700</p>  <p>Pareto Rank: 4 DB08339 6-(2,6-DICHL 46.6500 -7.0510</p>	<p>469717</p>  <p>Pareto Rank: 4 DB06236 Elvucitabine 46.7400 -6.6057</p>	<p>8515</p>  <p>Pareto Rank: 4 DB01782 2,6-Dihydro 46.9800 -6.4031</p>	<p>4293</p>  <p>Pareto Rank: 4 DB02986 N-(2-Thienyl 55.7100 -6.0923</p>

/home/claudias/ComplexIII/MOE/Pareto_Top20_1PPJ_1.mdb

Tue Feb 18 15:24:49 2020

Figure 17: Top 20 Pareto Ranking of 1PPJ

In the top 20 of the PDB 1SQP, myxothiazole was found in rank 2, picoxystrobin and MOA in rank 3 and kresoxim-I-dimethyl in rank 4. A positive success here was the recovery of myxothiazole with the drugbank ID DB04741 in rank 1.

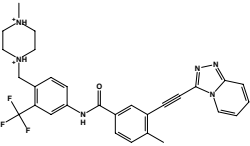
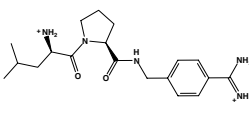
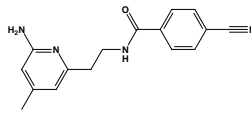
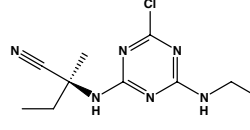
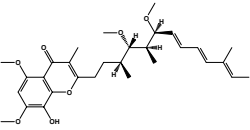
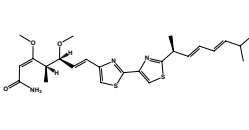
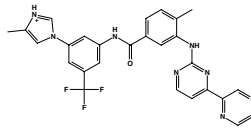
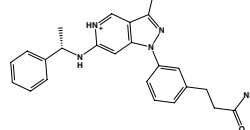
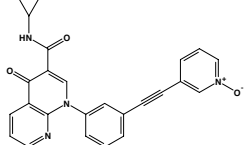
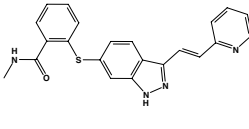
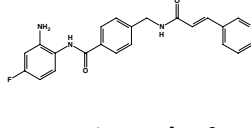
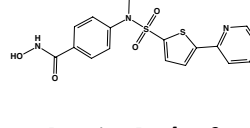
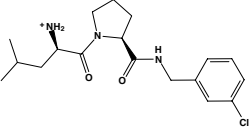
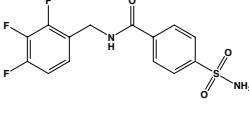
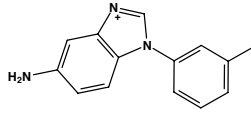
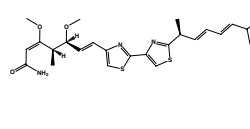
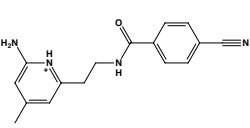
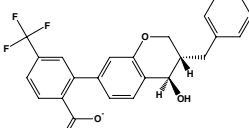
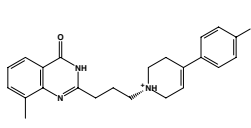
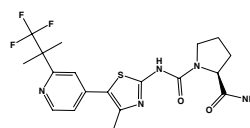
<p>10972974</p>  <p>Pareto Rank: 1 DB04741 Myxothiazol 38.5700 -12.2511</p>	<p>25220914</p>  <p>Pareto Rank: 1 DB06996 D-leucyl-N-(38.5900 -8.5968</p>	<p>10221335</p>  <p>Pareto Rank: 1 DB07389 N-[2-(6-AMIN 38.8000 -8.5808</p>	<p>449582</p>  <p>Pareto Rank: 1 DB07551 (2S)-2-([4-c 38.8700 -6.4898</p>
<p>10221335</p>  <p>Pareto Rank: 2 DB07389 N-[2-(6-AMIN 38.8000 -8.2431</p>	<p>Myxothiazol</p>  <p>Pareto Rank: 2 38.5600 -12.2200</p>	<p>24941249</p>  <p>Pareto Rank: 3 DB06963 3-[3-(3-meth 36.8500 -11.4241</p>	<p>5289085</p>  <p>Pareto Rank: 3 DB08330 METHYL (2Z)- 37.9400 -11.3120</p>
<p>71475839</p>  <p>Pareto Rank: 3 DB15396 PF-114 38.4700 -10.5757</p>	<p>1510981</p>  <p>Pareto Rank: 3 DB07972 1-(3-METHYLP 38.5600 -8.4913</p>	<p>176885</p>  <p>Pareto Rank: 3 DB06656 TAS-106 38.7500 -7.6980</p>	<p>7211</p>  <p>Pareto Rank: 3 DB13826 Etiohexadiol 38.7600 -4.7731</p>
<p>Picoxystrobin</p>  <p>Pareto Rank: 3 36.6600 -11.9145</p>	<p>MOA</p>  <p>Pareto Rank: 3 37.3500 -11.3176</p>	<p>24941248</p>  <p>Pareto Rank: 4 DB06897 3-[3-chloro- 36.8000 -11.3895</p>	<p>24941249</p>  <p>Pareto Rank: 4 DB06963 3-[3-(3-meth 36.8500 -11.1852</p>
<p>449013</p>  <p>Pareto Rank: 4 DB03220 FR233623 37.0100 -10.7904</p>	<p>56649450</p>  <p>Pareto Rank: 4 DB12015 Alpelisib 37.4500 -10.3179</p>	<p>6436135</p>  <p>Pareto Rank: 4 DB00587 Cinalukast 37.9400 -10.2872</p>	<p>24963048</p>  <p>Pareto Rank: 4 DB07812 N-[(1S)-2-am 38.0600 -9.9758</p>

/home/clauidias/ComplexIII/MOE/Pareto_Top20_1SQP_3.mdb

Tue Feb 18 16:36:37 2020

Figure 18: Top 20 Pareto Ranking of 1SQP

The top 20 of the PDB 1SQX resulted in a rank 1 for stigmatellin and myxothiazole out of the 30 inhibitors, as well as a rank 3 for myxothiazole with the drugbank ID DB04741.

<p>71475839</p>  <p>Pareto Rank: 1 DB15396 PF-114 38.4700 -10.5732</p>	<p>25220914</p>  <p>Pareto Rank: 1 DB06996 D-leucyl-N-(38.5900 -9.0224</p>	<p>10221335</p>  <p>Pareto Rank: 1 DB07389 N-[2-(6-AMIN 38.8000 -8.2613</p>	<p>449582</p>  <p>Pareto Rank: 1 DB07551 (2S)-2-[[4-c 38.8700 -6.0060</p>
<p>Stigmatellina</p>  <p>Pareto Rank: 1 38.0000 -10.9707</p>	<p>Myxothiazol</p>  <p>Pareto Rank: 1 38.5600 -10.0679</p>	<p>16063245</p>  <p>Pareto Rank: 2 DB12323 Radotinib 35.3600 -10.7971</p>	<p>24941249</p>  <p>Pareto Rank: 2 DB06963 3-[3-(3-meth 36.8500 -10.5626</p>
<p>9919680</p>  <p>Pareto Rank: 2 DB13029 MK-0873 37.0200 -10.5297</p>	<p>6450551</p>  <p>Pareto Rank: 2 DB06626 Axitinib 38.0300 -10.5086</p>	<p>12136798</p>  <p>Pareto Rank: 2 DB06334 Tucidinostat 38.0600 -9.9194</p>	<p>449096</p>  <p>Pareto Rank: 2 DB02917 N-Hydroxy-4- 38.2000 -9.6087</p>
<p>25113127</p>  <p>Pareto Rank: 2 DB06911 D-leucyl-N-(38.2500 -9.4103</p>	<p>446240</p>  <p>Pareto Rank: 2 DB04549 4-(Aminosulf 38.4400 -8.8691</p>	<p>1510981</p>  <p>Pareto Rank: 2 DB07972 1-(3-METHYLP 38.5600 -8.6702</p>	<p>10972974</p>  <p>Pareto Rank: 2 DB04741 Myxothiazol 38.5700 -8.3071</p>
<p>10221335</p>  <p>Pareto Rank: 2 DB07389 N-[2-(6-AMIN 38.8000 -8.1979</p>	<p>9823886</p>  <p>Pareto Rank: 3 DB13053 CP-195543 36.1900 -10.5385</p>	<p>448889</p>  <p>Pareto Rank: 3 DB03072 2-{3-[4-(4-F 36.7200 -10.5362</p>	<p>56649450</p>  <p>Pareto Rank: 3 DB12015 Alpelisib 37.4500 -10.4650</p>

/home/claudias/ComplexIII/MOE/Pareto_Top20_1SQX_withH.mdb

Tue Feb 18 15:46:06 2020

Figure 19: Top 20 Pareto Ranking of 1SQX

7 Conclusion

In this thesis, structure-based in silico methods were used to identify substances that may have mitochondrial toxicity. The first redocking attempts were successful except for azoxystrobin. Even with the change of the program and thus different calculation algorithms, the reproducibility of azoxystrobin was not successful. Unfortunately, it was not possible to find out why this inhibitor led to negative results in the docking experiments.

Another goal was to dock the existing inhibitors in the human complex. The high sequence identity of the human complex with the bovine and chicken complex suggests that already co-crystallized inhibitors should lead to the same binding results here as well. However, it turned out that it was not possible to carry out the docking process in both cytochrome b chains of the dimer. This raises the question to what extent the dimers of the human complex are identical. According to our sequence check, these should be identical. Because of that it cannot be explained why the docking experiments did not work in both chains. Furthermore, the desired interactions could not be successfully demonstrated in the human complex with all used inhibitors. In this work, chains of the protein were removed in order to accelerate the docking process; further docking attempts with the whole protein could possibly lead to different results. After all, it is known that there are three classes of inhibitors and that these cause different conformations of the protein.

The preparation of the pharmacophore turned out to be difficult because the inhibitors have very different structures. The binding pocket is unfortunately very far out in the membrane, so that the outer area is very spacious. In both binding pockets, hydrophobic properties predominate, such as Ar-Ar interactions or π -interactions, whereby specific interactions such as hydrogen bonds could only be defined in the head region.

It was therefore necessary to create 2 pharmacophores for each binding pocket, with which the screening was carried out.

Thanks to machine learning, the respective hit lists could be linked to one another and evaluated in Knime. The Pareto ranking made it possible to assign substances to different ranks, rank 1 containing the best docking scores and pharmacophore fit scores, which in turn indicate a high specificity as an inhibitor.

8 References

1. Ames BN., Atamna H., Killilea DW. Mineral and vitamin deficiencies can accelerate the mitochondrial decay of aging. *Molecular Aspects of Medicine* 2005;**26**(4):363–78. Doi: 10.1016/j.mam.2005.07.007.
2. Rich PR., Maréchal A. The mitochondrial respiratory chain. *Essays Biochem* 2010;**47**:1–23. Doi: 10.1042/bse0470001.
3. Lill R., Diekert K., Kaut A., Lange H., Pelzer W., Prohl C., et al. The Essential Role of Mitochondria in the Biogenesis of Cellular Iron-Sulfur Proteins 1999;**380**(10):1157–66. Doi: 10.1515/BC.1999.147.
4. Annesley SJ., Fisher PR. Mitochondria in Health and Disease. *Cells* 2019;**8**(7):680. Doi: 10.3390/cells8070680.
5. Benard G., Bellance N., Jose C., Rossignol R. Relationships Between Mitochondrial Dynamics and Bioenergetics, 2011, p. 47–68.
6. Wittig I., Schägger H. Supramolecular organization of ATP synthase and respiratory chain in mitochondrial membranes. *Biochimica et Biophysica Acta (BBA) - Bioenergetics* 2009;**1787**(6):672–80. Doi: 10.1016/j.bbabi.2008.12.016.
7. Esser L., Quinn B., Li Y-F., Zhang M., Elberry M., Yu L., et al. Crystallographic Studies of Quinol Oxidation Site Inhibitors: A Modified Classification of Inhibitors for the Cytochrome bc₁ Complex. *Journal of Molecular Biology* 2004;**341**(1):281–302. Doi: 10.1016/j.jmb.2004.05.065.
8. Esser L., Zhou F., Zhou Y., Xiao Y., Tang W., Yu C-A., et al. Hydrogen Bonding to the Substrate Is Not Required for Rieske Iron-Sulfur Protein Docking to the Quinol Oxidation Site of Complex III. *J Biol Chem* 2016;**291**(48):25019–31. Doi: 10.1074/jbc.M116.744391.
9. Berry EA., Huang L-S. Conformationally linked interaction in the cytochrome bc₁ complex between inhibitors of the Q_o site and the Rieske iron–sulfur protein. *Biochimica et Biophysica Acta (BBA) - Bioenergetics* 2011;**1807**(10):1349–63. Doi: 10.1016/j.bbabi.2011.04.005.
10. Guo R., Zong S., Wu M., Gu J., Yang M. Architecture of Human Mitochondrial Respiratory Megacomplex I2III2IV2. *Cell* 2017;**170**:1247-1257.e12. Doi: 10.2210/pdb5xte/pdb.
11. Gao X., Wen X., Esser L., Quinn B., Yu L., Yu C-A., et al. Structural Basis for the Quinone Reduction in the bc₁ Complex: A Comparative Analysis of Crystal Structures of Mitochondrial Cytochrome bc₁ with Bound Substrate and Inhibitors at the

- Qi Site,. *Biochemistry* 2003;**42**(30):9067–80. Doi: 10.1021/bi0341814.
12. Berry EA., Huang L., Lee D-W., Daldal F., Nagai K., Minagawa N. Ascochlorin is a novel, specific inhibitor of the mitochondrial cytochrome bc1 complex. *Biochim Biophys Acta* 2010;**1797**(3):360. Doi: 10.1016/j.bbabi.2009.12.003.
13. Parasuraman S. Protein data bank. *J Pharmacol Pharmacother* 2012;**3**(4):351. Doi: 10.4103/0976-500X.103704.
14. Gao X., Wen X., Yu CA., Esser L., Tsao S., Quinn B., et al. The Crystal Structure of Mitochondrial Cytochrome bc1 in Complex with Famoxadone: The Role of Aromatic-Aromatic Interaction in Inhibition. *Biochemistry* 2003;**41**:11692–702. Doi: 10.2210/pdb1I0I/pdb.
15. Huang L-S., Cobessi D., Tung EY., Berry EA. Binding of the respiratory chain inhibitor antimycin to the mitochondrial bc1 complex: a new crystal structure reveals an altered intramolecular hydrogen-bonding pattern. *J Mol Biol* 2005;**351**(3):573–97. Doi: 10.1016/j.jmb.2005.05.053.
16. Esser L., Gong X., Yang S., Yu L., Yu C-A., Xia D. Surface-modulated motion switch: Capture and release of iron–sulfur protein in the cytochrome bc1 complex. *Proc Natl Acad Sci U S A* 2006;**103**(35):13045–50. Doi: 10.1073/pnas.0601149103.
17. Amporndanai K., Johnson RM., O'Neill PM., Fishwick CWG., Jamson AH., Rawson S., et al. X-ray and cryo-EM structures of inhibitor-bound cytochrome bc 1 complexes for structure-based drug discovery. *IUCrJ* 2018;**5**(Pt 2):200–10. Doi: 10.1107/S2052252518001616.
18. McPhillie M., Zhou Y., El Bissati K., Dubey J., Lorenzi H., Capper M., et al. New paradigms for understanding and step changes in treating active and chronic, persistent apicomplexan infections. *Sci Rep* 2016;**6**. Doi: 10.1038/srep29179.
19. Capper MJ., O'Neill PM., Fisher N., Strange RW., Moss D., Ward SA., et al. Antimalarial 4(1H)-pyridones bind to the Qi site of cytochrome bc1. *Proc Natl Acad Sci U S A* 2015;**112**(3):755–60. Doi: 10.1073/pnas.1416611112.
20. Nilsen A., LaCrue AN., White KL., Forquer IP., Cross RM., Marfurt J., et al. Quinolone-3-Diarylethers: A new class of drugs for a new era of malaria eradication. *Sci Transl Med* 2013;**5**(177):177ra37. Doi: 10.1126/scitranslmed.3005029.
21. David Hong W., Leung SC., Amporndanai K., Davies J., Priestley RS., Nixon GL., et al. Potent Antimalarial 2-Pyrazolyl Quinolone bc1 (Qi) Inhibitors with Improved Drug-like Properties. *ACS Med Chem Lett* 2018;**9**(12):1205–10. Doi: 10.1021/acsmchemlett.8b00371.

22. Hao G-F., Wang F., Li H., Zhu X-L., Yang W-C., Huang L-S., et al. Computational Discovery of Picomolar Qo Site Inhibitors of Cytochrome bc₁ Complex. *J Am Chem Soc* 2012;**134**(27):11168–76. Doi: 10.1021/ja3001908.
23. Zhang Z., Huang L., Shulmeister VM., Chi Y-I., Kim KK., Hung L-W., et al. Electron transfer by domain movement in cytochrome bc₁. *Nature* 1998;**392**(6677):677–84. Doi: 10.1038/33612.
24. Berry EA., Huang L., Lee D-W., Daldal F., Nagai K., Minagawa N. Ascochlorin is a novel, specific inhibitor of the mitochondrial cytochrome bc₁ complex. *Biochim Biophys Acta* 2010;**1797**(3):360. Doi: 10.1016/j.bbabi.2009.12.003.
25. Becker W f., Von Jagow G., Anke T., Steglich W. Oudemansin, strobilurin A, strobilurin B and myxothiazol: new inhibitors of the bc₁ segment of the respiratory chain with an E- β -methoxyacrylate system as common structural element. *FEBS Letters* 1981;**132**(2):329–33. Doi: 10.1016/0014-5793(81)81190-8.
26. von Jagow G., Link TA. Use of specific inhibitors on the mitochondrial bc₁ complex. *Methods Enzymol* 1986;**126**:253–71. Doi: 10.1016/s0076-6879(86)26026-7.
27. Zhu X., Zhang M., Liu J., Ge J., Yang G. Ametoctradin is a potent Qo site inhibitor of the mitochondrial respiration complex III. *J Agric Food Chem* 2015;**63**(13):3377–86. Doi: 10.1021/acs.jafc.5b00228.
28. Dreinert A., Wolf A., Mentzel T., Meunier B., Fehr M. The cytochrome bc₁ complex inhibitor Ametoctradin has an unusual binding mode. *Biochimica et Biophysica Acta (BBA) - Bioenergetics* 2018;**1859**(8):567–76. Doi: 10.1016/j.bbabi.2018.04.008.
29. Nilsen A., LaCrue AN., White KL., Forquer IP., Cross RM., Marfurt J., et al. Quinolone-3-Diarylethers: A new class of drugs for a new era of malaria eradication. *Sci Transl Med* 2013;**5**(177):177ra37. Doi: 10.1126/scitranslmed.3005029.
30. Pei J., Kim B-H., Grishin NV. PROMALS3D: a tool for multiple protein sequence and structure alignments. *Nucleic Acids Res* 2008;**36**(7):2295–300. Doi: 10.1093/nar/gkn072.
31. About UniProt. Available from: <https://www.uniprot.org/help/about> [accessed October 15, 2021].
32. *The latest release of DrugBank Online (version 5.1.8, released 2021-01-03)*, n.d.
33. Wishart DS., Feunang YD., Guo AC., Lo EJ., Marcu A., Grant JR., et al. DrugBank 5.0: a major update to the DrugBank database for 2018. *Nucleic Acids Research* 2018;**46**(D1):D1074–82. Doi: 10.1093/nar/gkx1037.

34. Pagadala NS., Syed K., Tuszynski J. Software for molecular docking: a review. *Biophys Rev* 2017;**9**(2):91–102. Doi: 10.1007/s12551-016-0247-1.
35. Maestro User Manual n.d.:478.
36. Glide User Manual n.d.:138.
37. GOLD User Guide n.d.:(2019 CSD Realease Update 3):220.
38. GOLD: Protein-Ligand Docking Software - The Cambridge Crystallographic Data Centre (CCDC). Available from: <https://www.ccdc.cam.ac.uk/solutions/csd-discovery/components/gold/> [accessed October 28, 2021].
39. LigandScout User Manual n.d.:143.

9 Appendix

9.1 List of Figures

Figure 1: Complexes of the mitochondrial Respiratory chain ⁵	1
Figure 2: human dimer bc1-complex with the three essentials catalytic	2
Figure 3: View of the dimeric cyt b and ISP in the bc1-complex ⁷	3
Figure 4: Q-cycle mechanism ⁸	4
Figure 5: Steps of the Thesis	6
Figure 6: human complex with both binding sides	23
Figure 7: PDB 1SQX with the co-crystalized inhibitor Stigmatellin and the h-bond to Glu271	23
Figure 8: Qo-binding side of the human complex and the most important side chains are labeled.....	24
Figure 9: Qi-binding side of the human complex with the most important residues..	24
Figure 10: Comparison of the PDBs identity between cyt. b of bovine and human complex	25
Figure 11: Comparison of the PDBs identity between cyt. b of chicken and human complex	26
Figure 12: Docking Result of Azoxystrobin (green from docking, orange from PDB) in GOLD	28
Figure 13 Qo-site pharmacophore 1	32
Figure 14 Qo-site pharmacophore 2	32
Figure 15 Qi-site both pharmacophores.....	33
Figure 16: Knime workflow for the Qo binding site with the PDB of 1SQP	34
Figure 17: Top 20 Pareto Ranking of 1PPJ.....	35
Figure 18: Top 20 Pareto Ranking of 1SQP.....	36
Figure 19: Top 20 Pareto Ranking of 1SQX.....	37

9.2 List of Tables

Table 1: Crystal structures of bos taurus bc1-complex with inhibitors divided in the two binding site modes	9
Table 2: Crystal structures of Gallus gallus bc1-complexe with inhibitors.....	10
Table 3: Crystal structures of the Yeast bc1-complexe with inhibitors	10
Table 4: Structures of the 30 inhibitors.....	16

Table 5: Sequences of the bc1-complex from the various species	22
Table 6: Comparison of the two binding sites of the most important amino acids	25
Table 7: used PDBs for the Qo-Site Redocking	26
Table 8: used PDBs for the Qi-Site Redocking	27

9.3 List of Abbreviations

ATP	Adenosine-triphosphate
CIII	Complex III of the respiratory chain
Cyt b	Cytochrome b
d.s.	Docking score
ELQ271	Quinolone derivative, 2-methylquinolin-4(1H)-one in which the hydrogen at position 3 is replaced by a 4-[4-(trifluoromethoxy)phenoxy]phenyl group.
GSK932121	3-chloro-6-(hydroxymethyl)-2-methyl-5-{4-[3-(trifluoromethoxy)phenoxy]-phenyl}pyridin-4-ol
GW844520	potent anti-malarial compound, 3-chloro-2,6-dimethyl-5-{4-[4-(trifluoromethoxy)phenoxy]phenyl}pyridin-4-ol
HHDBT	5-Heptyl-6-Hydroxy-1,3-Benzothiazole-4,7-Dione
MOAS	Methoxy Acrylate Stilbene; UPAC: 3-methoxy-2-(2-styryl-phenyl)-acrylic acid methyl ester)
MJM	(4aS)-2-methyl-3-(4-phenoxyphenyl)-5,6,7,8-tetrahydroquinolin-4(4aH)-one
NQNO	2-N-Nonyl-4-hydroxyquinoline-N-oxide
PDB	Protein Databank
Q _{o/N}	binding site on the outer mebrane or negative site
Q _{i/P}	binding site on the inner mebrane or positive site
UHDBT	4-hydroxy-5undecyl-1,3-benzothiazole-6,7-dione
JG144	(5S)-3-3Anilino-5-(2,4-difluorophenyl)-5-methyl-1,3-oxazolidine-2,4-dione
SCR0911	7-methoxy-3-methyl-2-[5-[4-(trifluoromethoxy)phenyl]pyridin-3-yl]-1~{H}-quinolin-4-one
WDH2G7	7-methoxy-3-methyl-2-[1-[4-(trifluoromethoxy)phenyl]methyl]pyrazol-4-yl]-3~{H}-quinolin-4-one